Mutual insight on ferroelectrics and hybrid halide perovskites: a platform for future multifunctional energy conversion

Richa Pandey, Gaurav Vats, Jae Yun, Chris R Bowen, Anita W. Y. Ho-Baillie, Jan Seidel, Keith Tobias Butler and Sang-Il Seok

Published version information

This is the peer reviewed version of the following article:

Citation: R Pandey et al. "Mutual insight on ferroelectrics and hybrid halide perovskites: a platform for future multifunctional energy conversion." Advanced Materials, vol. 31, no. 43 (2019): 1807376.

DOI: 10.1002/adma.201807376

Mutual insight from ferroelectric and hybrid halide perovskites: A platform for future multifunctional energy conversion

Richa Pandey[#], *Gaurav Vats*[#,*], *Jae Yun, Chris R Bowen, Anita W. Y. Ho-Baillie, Jan Seidel*[*], *Keith Tobias Butler and Sang-II Seok*[*]

Richa Pandey
Centre of Excellence in Nanoelectronics, Indian Institute of Technology Bombay, Powai 400076, India and Centre for Research in Nanotechnology and Science, Indian Institute of Technology Bombay, Powai 400076, India
Gaurav Vats and Prof. Jan Seidel,
School of Materials Science and Engineering, University of New South Wales, Sydney 2052, Australia
Email: g.vats@unsw.edu.au ; jan.seidel@unsw.edu.au
Dr. Jae Yun and Prof. Anita W. Y. Ho-Baillie
Australian Centre for Advanced Photovoltaics, School of Photovoltaic and Renewable Energy Engineering, University of New South Wales, Sydney 2052, Australia
Prof. Chris R Bowen
Materials Research Centre, Department of Mechanical Engineering, University of Bath, Bath BA2 7AY, United Kingdom
Dr. Keith Tobias Butler
ISIS Facility, Rutherford Appleton Laboratory, Harwell Oxford Didcot, Oxfordshire OX11 0QX, United Kingdom
Prof. Sang-II Seok[*]
School of Energy and Chemical Engineering, Ulsan National Institute of Science and Technology (UNIST) UNIST-gil 50, Ulsan 689-798, South Korea.
*Email:seoksi@unist.ac.kr

[#]Authors contributed equally.

Keywords: Perovskites, photoferroic effect, pyroelectric effect, ferroelectrics, thermo-electric effect, energy storage

This review provides insights, analogies and future prospects of both organic-inorganic hybrid halide perovskites and inorganic perovskites for next generation multifunctional energy

conversion and storage devices. Recent advancements have highlighted the potential of hybrid perovskites for high-efficiency solar cells. The intrinsic polar properties of these materials, including the potential for ferroelectricity, provide additional possibilities for simultaneously exploiting several other energy conversion mechanisms such as the piezoelectric effect, pyroelectric effect, thermal energy conversion, thermoelectric effect and electrical energy storage. These additional properties can support the performance of perovskite solar cells, and energy conversion using these effects (piezo-, pyro-, and thermoelectric effect) could also be enhanced by a change in light intensity. Thus, there lies a range of possibilities for tuning the structural, electronic, optical and magnetic properties of perovskites to simultaneously harvest energy using more than one mechanism to realize an improved efficiency. This requires a basic understanding of concepts, mechanisms, corresponding material properties and the underlying physics involved with these effects. In this context, this review provides an insight into the analogies, state-of-the-art technologies, concepts and prospects under the umbrella of perovskite materials in order to stimulate novel directions of research in the area of solid-state energy conversion. Often, these approaches are considered to be entirely different branches of research, however considering them simultaneously and holistically can provide several new opportunities.

1. Introduction

Perovskites are materials with an ABX_3 type structure where A and B are cations of different atomic radii that occupy the corner and center of the unit cell, respectively, whereas X is an anion which is coordinated with B located at the face of the unit cell to form BX_6 octahedra; see Figure 1(a) and (b). The coordination number of the A cation is 12, which is the largest possible number of nearest neighbors and a unique feature of the perovskite structure. Perovskites can be classified based on their band gap as conductors and insulators/dielectrics. Dielectrics with a band gap less than 3eV are termed *semiconductors*. These can also be

classified as centrosymmetric, asymmetric and non-centrosymmetric based on their symmetry. Non-centrosymmetric perovskites that possess a spontaneous polarization that can be fully switched by application of an external electric field, stress, thermal fluctuation or light (as illustrated in Figure 1 (b)-(c)) are classified as *ferroelectrics*. The phenomena of achieving a change in polarization by means of thermal fluctuations is known as the 'pyroelectric effect' while a change in polarization by exposure to light and stress is termed the 'photoferroic effect' and 'piezoelectric effect' respectively. It is to be noted that all ferroelectrics are both pyroelectric and piezoelectric in nature, while the reverse is not true. At the same time, there exists a group of perovskites (semiconducting hybrid organic-inorganic halide perovskites) which may or may not be non-centrosymmetric but have appealing charge generation and transport properties which leads to a significant 'photovoltaic' response; namely the effect of obtaining an electrical output on exposure to light. Figure 2 provides an insight into the relationship between these materials and suggests that a single material could have the both ferroelectric and semiconducting nature. A coexistence of these features could be utilized for enhanced energy conversion and storage. Thus, it will be of interest to explore the possibilities of simultaneously harnessing energy from different sources and distinct mechanisms using a single perovskite material.

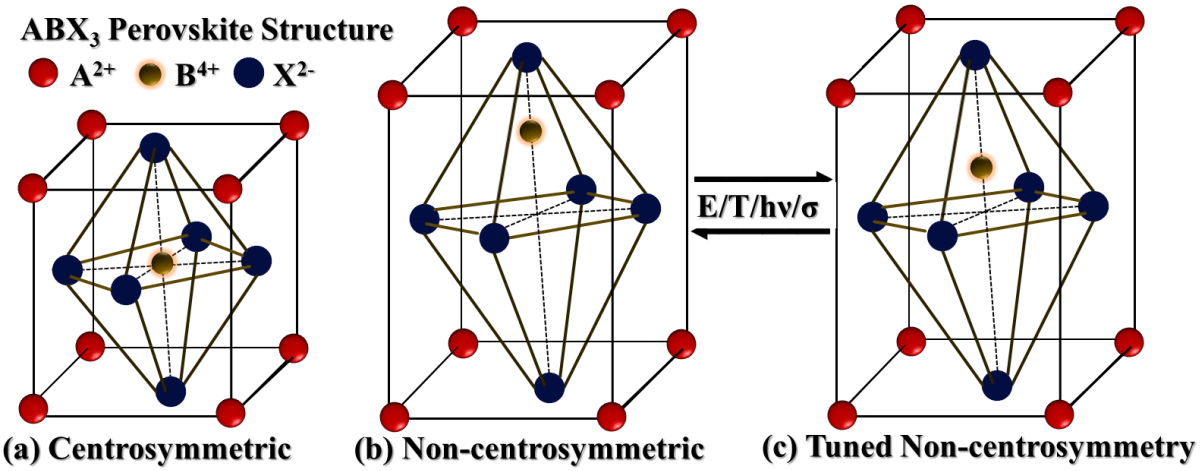

Figure 1: (a) Perovskite structure with symmetric and (b) non-centrosymmetric arrangements. (b)-(c) tuning of the degree of non-centrosymmetry by means of an external stimulus, where *E*

is electric field, T is temperature, hv is the photon energy (h is the Planck's constant and v is the frequency of the incident light) and σ is the stress.

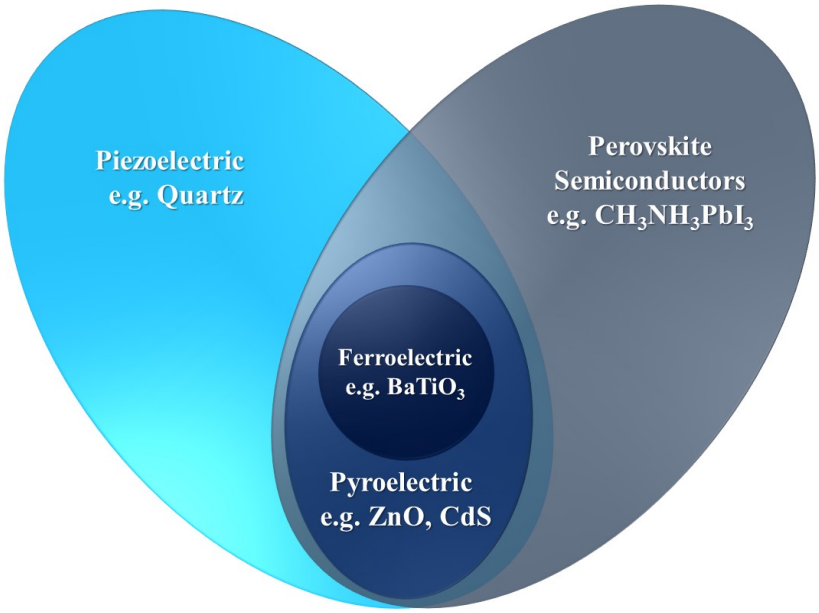

Figure 2: Relationships between perovskite, piezoelectric, pyroelectric and ferroelectric materials

In this context, two classes (organic-inorganic hybrid perovskites and inorganic ferroelectric perovskites) of perovskites focused on in this review are well established in their respective domains. On the one end hybrid perovskites are well known for their photovoltaic response[1-6] with existing research focusing on understanding their behavior on the basis of their crystal structure in order to design improved materials [7-9]; while on the other hand perovskite ferroelectrics, another special class of perovskites, are well known for piezoelectric, pyroelectric and thermal energy conversion systems[10-36], and are also gaining interest as photovoltaic and optoelectronic materials[37-50]. Intriguingly, both hybrid perovskites and ferroelectrics are also being investigated for thermoelectric applications[51, 52]. Therefore, the possibilities of utilizing this class of materials to provide multiple functionalities using a single material for a more desirable energy output is worthy of consideration. Figure 3 indicates the classification scheme for perovskites and highlights the area of interest. The chosen area of interest is directly related to the electrical (dielectric or semi-conducting) and

ferroelectric properties of perovskites. Therefore, it becomes vital to understand these features before simultaneous consideration of both ferroelectric and hybrid halide perovskites for any application. The present review aims to motivate scientific community either to tune the semi-conducting features (band-gap and charge transport properties) of ferroelectrics or to induce ferroelectricity in hybrid halide perovskites from a better understanding of the structural analogy in context of the device needs. Once the device needs are understood the properties could then be tuned by taking into account the tolerance factor.

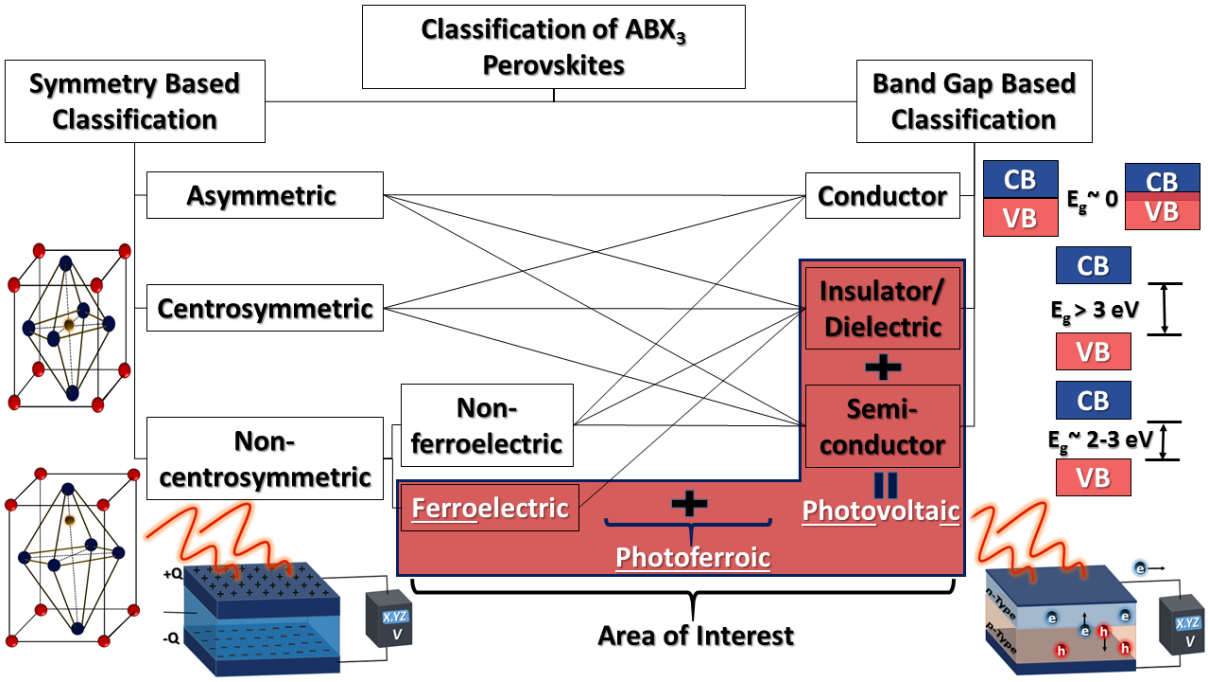

Figure 3: Classification of perovskites for multifunctional energy harvesting using a single engineered material.

Goldschmidt's tolerance factor ($t = (r_A + r_X)/ \sqrt{2}\,(r_B + r_X)$)[53] helps in estimating the degree of distortion which is applicable at room temperature to the empirical ionic radii (r_A, r_B and r_X). The ideal perovskite-type structure is cubic with space group Pm-3m[54] and is expected to have a tolerance factor of unity. However, both ferroelectric and hybrid halide perovskites are found to have lower *t*-values ($0.75 < t < 1.0$). *t*-values help in governing and tuning the presence of ferroelectricty in perovskites[7] and are responsible for the transition temperatures in ferroelectrics[55]. In the case of hybrid organic-inorganic perovskites, the A-site and/or X-

site ions are replaced by molecular building blocks, hence, the tolerance factor is adapted to the following equation: $t = (r_{Aeff} + r_{xeff})/ \sqrt{2} (r_B + h_{xeff}/2)$[56, 57], where r_B defines the Shannon ionic radius of the B-site metal ion, r_{Aeff} denotes the effective radius of the A-site cation, and r_{Xeff} and h_{Xeff} denote the effective radius and length of the X-site molecular ions, respectively. Understanding of the effects of tuning these radii could help in controlling the semiconducting and ferroelectric features of the perovskites.

2. Electrical properties of perovskites

As described above, hybrid perovskites are semi-conducting in nature while ferroelectrics can be insulating, or semi-conducting based on their band gap. The electrical properties of perovskites are primarily dependent on their crystal structure (symmetry) and electronic structure. The crystal structure is responsible for the moment of dipoles while the electronic structure governs the surface charges as well as ionic and electronic conductivities which are responsible for the overall material behavior. The most important properties of perovskites include charge transport, ferroelectricity and dielectric/semi-conducting behavior.

2.1. Charge transport properties

2.1.1. Charge transport in ferroelectric perovskites

The charge transport properties of perovskites are controlled by mobilities, diffusion lengths, effective masses and lifetime of the charge carriers.[58, 59] Ferroelectric perovskites typically have short carrier diffusion lengths and lifetimes due to their high band gap[59] and hence have poor charge transport properties in contrast to hybrid halide perovskites ferroelectrics.[58, 59] However, the presence of dipoles, domains and boundaries facilitates charge separation.[60] The presence of surface charges, ions, dipoles and electrons make it difficult to conclude the actual conduction mechanism in ferroelectrics. However, in general, charge transport in ferroelectric perovskites stems either from or a combination of bulk (Poole–Frenkel emission,

Ohmic conduction, charge carrier hopping, space charge conduction) or/and interface (Schottky emission and Fowler–Nordheim tunneling) effects.[58, 61] Additionally, charge screening at domain walls and conduction through domains plays an important role in governing the charge transport properties, especially in ferroelectric thin films.[62-64] Diffusion of oxygen vacancies and change in oxidation state of central atoms due to the presence of oxygen vacancies have also been reported as the assisting mechanisms for better transport properties.[49, 50, 65, 66] The transport properties in ferroelectrics could further be tuned by heat-treatment and strain engineering which eventually leads to defect induced conduction.[67]

2.1.2. Charge transport in hybrid halide perovskites

The transport properties of hybrid halide perovskites are dependent on defects, intrinsic doping, carrier concentrations and spin-orbit coupling; these factors have been reviewed in detail by Brenner *et. al.*[68]. One of the most striking features of hybrid halide perovskite is the long lifetime of the carriers generated. Even though the absorber layers are typically deposited using a simple process with little control of film quality and defect concentrations, reasonable photovoltaic efficiencies (> 10 %) can be maintained. One reason suggested for this apparent acceptance of defects is a result of the so-called “defect tolerant” electronic structure.[69] Simply stated, defect tolerance arises when the orbital hybridization in the material gives rise to band edges that do not result in deep traps when defects are formed. For example, an anti-bonding valence band edge results in an electronic state below or close to the band edge, if a dangling bond is formed.[70] This absence of deep states can account for reduced recombination, due to the reduced trapping of carriers as shown by Shockley-Reed-Hall theory. Whilst this can explain some of the reduced recombination rates, there are other factors related to ferroelectricity that could be at play. For example, ferroelectric domains can contribute to increased dielectric screening (section 2.2), which reduces carrier cross-sections for recombination, and electric fields at the Pb centres can induce splitting of the conduction

band edge that could suppress band-to-band recombination rates (see section 2.1.3). One recent report has also revealed the presence of ferroelastic domains in hybrid halide perovskite $CH_3NH_3PbI_3$, which could be correlated to light induced chemical segregation and its elastic behavior.[71]

Theoretical analysis of the band structure of hybrid halide perovskite $CH_3NH_3PbI_3$ ($MAPI_3$) reveals that the conduction (and to a much lesser extent valence) band edges have extrema, which occur slightly removed from the special high-symmetry points of the Brillouin zone. The origin of this asymmetry has been shown to be Rashba splitting, where a finite local electric field interacts with the spin-orbit component of the orbitals to lift the degeneracy of band extrema at special points and split the minimum/maximum in momentum space. The result of this splitting is that the band-gap has indirect characteristics.[72-75] It has been calculated that under low doping densities and modest illumination, $MAPI_3$ exhibits an indirect gap.[76] A comparison of the radiative recombination rate with a direct bandgap (ignoring the effect of Rashba splitting) with an indirect bandgap (including the effect of Rashba splitting), reveals that it is suppressed by 350 times in the later scenario. Molecular dynamics simulations have shown that this Rashba splitting persists in dynamic crystals,[77] demonstrating that it can play an important role in observed enhanced carrier lifetimes. Recent experimental studies demonstrated how removing Rashba splitting, by applying pressure to the sample, results in greatly increased radiative recombination rates, adding confidence to the hypothesis that band splitting is important for enhanced carrier lifetimes.[76]

2.2. Dielectric/semi-conducting properties

The dielectric property of a material is a result of the surface charge *(P_{SC})*, dipolar *(P_{dp})*, ionic *(P_{ionic})* and electronic *($P_{electronic}$)* polarizations. These polarizations are frequency dependent and can be easily distinguished by relaxation on increasing the frequency in the following

order: P_{SC}, P_{dp}, P_{ionic}, $P_{electronic}$. Relaxation occurs due to a variation in the effective masses of the charge carriers associated with these polarizations. The dielectric constant of any material can also be expressed as a combination (ε'-$i\varepsilon''$) of real (ε') and imaginary (ε'') parts, where the real part represents the energy storage capability while the imaginary part denotes the associated energy losses. An increase in imaginary part on exposure to an external stimulus indicates a semiconducting behavior whereas an increase in the real part denotes a dielectric response. Therefore, a light and frequency dependent change in dielectric constant can help in understanding whether the material's behavior is governed by semiconducting or dipolar features which can further be helpful in identifying the presence of ferroelectricity and associated features. An increase in imaginary part or a decrease in real part of the dielectric constant on exposure to light at high frequencies is a clear indication of light induced charge carriers (electrons and holes) and can be considered as a technique to reveal charge transport properties, as also reported[78] in the case of hybrid perovskites. Based on the same idea, nanoscale measurements (Kelvin probe force microscopy (KPFM) and piezoresponse force microscopy (PFM)) could be performed to confirm ion migration in hybrid perovskites.

2.3. Ferroelectricity

The delicate balance of forces between the species that form the material determines the structure of a crystal. In polar materials, there is a competition between Coulombic, Pauli and covalent forces. If one considers the lattice as being comprised of point charges, the Coulomb interaction favors the condensation of all charges to a neutral singularity; this is counterbalanced by Pauli repulsion between the electron clouds of the ions. In the absence of competing forces, the balance of Pauli repulsion and Coulomb attraction would lead to the formation of symmetric structures, with no finite electric dipole.[79] However, additional covalent bonding interactions can lead to small distortions of the symmetric lattice, which

induce a local dipole moment, giving rise to ferroelectricity. There are several well-known mechanisms by which ferroelectricity has been shown to arise in low temperature phases of oxide perovskites (and perovskite derivatives, such as the Dion-Jacobson and Ruddlesden-Popper phases).

2.3.1. Proper ferroelectricity

Proper ferroelectrics are a class of materials where the spontaneous polarization is driven by Brillouin zone centre lattice instability (soft modes at the Gamma point)[80]. This is the case in $PbTiO_3$ and $BaTiO_3$, where the Ti ion at the centre of the BX_6 octahedra spontaneously moves off centre as the temperature is decreased. Although there is some debate as to whether this movement off centre is as a result of a soft mode, or an order-disorder transition,[81] the chemical origin of the asymmetry is clear. In this case the valence band edge of the material is dominated by oxygen *2p* orbitals. The movement of Ti off the octahedral centre is driven by a hybridization of the empty *d*-states of the Ti(IV) ion with the O *2p* states, in a second-order Jahn-Teller distortion.[82] In the case of $PbTiO_3$ there is further hybridization of the Pb(IV) *d*-states with the oxygen, giving a final rhombohedral phase, in $BaTiO_3$ there is no such further hybridization and the final phase is rhombohedral.[82] This kind of ferroelectricity is difficult in Pb based hybrid perovskites, as the Pb (II) ion at the centre of the octahedra does not have the empty d^0 orbitals, which result in the second-order Jahn-Teller effect.

2.3.2. Stereo active ferroelectricity

Ferroelectricity has also been shown to be driven by the presence of a so-called stereo active lone pair, as in $BiFeO_3$.[83] In this case the polar distortion is driven by the A-site moving off centre, to facilitate hybridization of the Bi *6s* lone pair and the oxygen orbitals. Lone pairs on the B-site have also been shown to result in ferroelectric distortions in $CsPbF_3$ where Pb is in the (II) oxidation state.[84] It has been suggested that lone-pair driven distortions could contribute to ferroelectricity in hybrid-halide perovskites, however there is no evidence to

date of any stereo-activity in the lone pairs of $MAPbI_3$. The most likely source of any ferroelectricity in $MAPbI_3$, is the MA^+ organic cation, which carries a local dipole of 2.29 D.[85] This idea was initially proposed theoretically and was subsequently supported by results from neutron diffraction experiments. The MA^+ ion, which rotates freely in the cubic phase, becomes locked in as the temperature is decreased. In the low temperature orthorhombic phase the MA ion has been shown to adopt an anti-ferroelectric structure, with alternating lines of the molecular dipoles oriented in opposite directions[86, 87]. However, the orientation and existence of ferroelectric ordering of the molecules at higher temperatures, relevant to solar cell operation, has proven more difficult to ascertain. Recently there have been some more conclusive reports, demonstrating that whether halide perovskites are ferroelectric or not is dependent on the identity of the halide; while $MAPbBr_3$ is shown not to be ferroelectric,[88] $MAPbI_3$ is shown to be ferroelectric in its tetragonal room temperature phase.[89] However, a more important question is what can be gained from the presence of ferroelectricity in any perovskite. The presence of ferroelectricity is a confirmation of additional features of piezoelectricity and pyroelectricity. It is to be noted that a ferroelectric material needs to be poled in order to explore piezo- and pyro-electric features as these are dependent on remnant polarization. Simultaneous utilization of these effects could lead to a true multifunctional device which is likely to work beyond the predicted individual limits of ferroelectrics and hybrid halide perovskites.

3. Additional functionalities due to ferroelectricity

3.1. Pyroelectricity

The ability of generating an electrical potential due to changes in the state of polarization as a result of thermal fluctuations is known as the *pyroelectric effect*[28, 34, 90, 91]. This generated potential could further be utilized to obtain an electrical current through an external circuit.

Figure 4 shows the schematic of time dependent thermal fluctuations that lead to a displacement of the central ion in a non-centrosymmetric perovskite and results in a change in output voltage. It is to be noted that the mechanisms (in addition to non-centrosymmetric distortion) explained in the previous section could also lead to pyroelectric effect in perovskites. This can be used to supply an electrical current using a resistive load. The change in polarization (ΔP_i) with temperature change (ΔT) is given as[92]:

$$\Delta P_i = p\Delta T \tag{1}$$

where, p is the pyroelectric coefficient perpendicular to direction of the electrodes (i.e. in the polarization direction). Further, for a given surface area A, the induced short circuit current (I_P) for a given rate of temperature change (dT/dt) is[92, 93]

$$I_P = Ap\frac{dT}{dt} \tag{2}$$

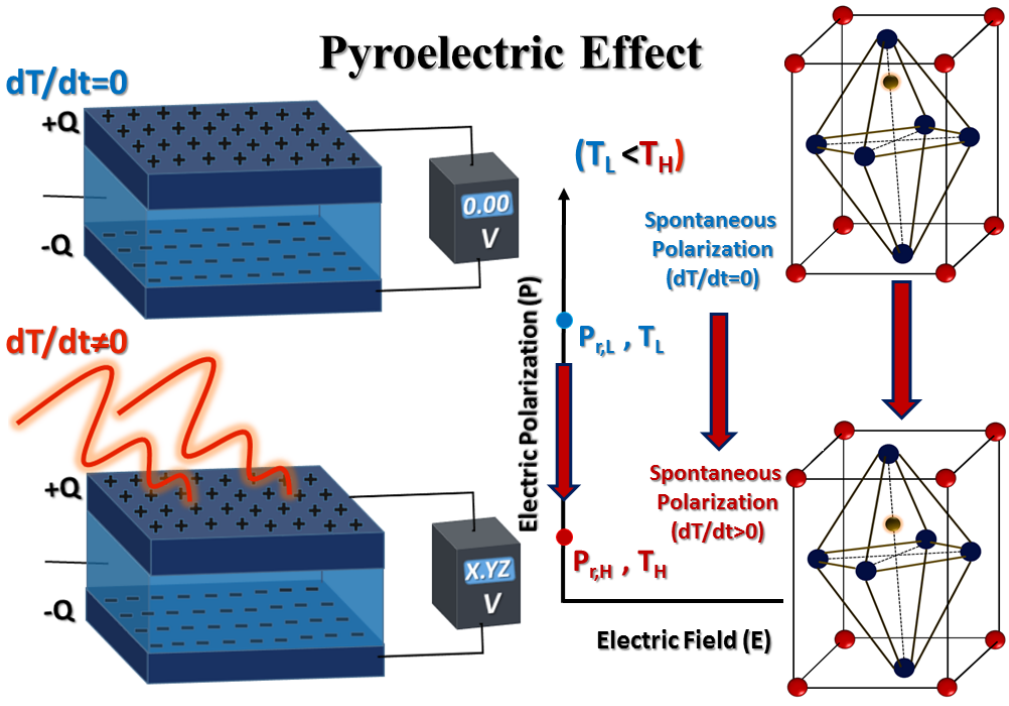

Figure 4: Schematic of pyroelectric effect where time dependent thermal fluctuations cause the displacement of the central atom in a non-centrosymmetric perovskite and results in an output voltage.

3.2. Piezoelectricity

Piezoelectricity can be defined as the linear coupling between stress and polarization[18] and piezoelectric materials undergo a polarization change when mechanical stresses are applied.[18] This change of polarization lead to an induced electrical current, which could further be extracted through an external circuit.[18] The potential energy *(QV)* per unit charge generation *(Q)* due to stress induced dipole movement can be expressed as the generated potential difference *(V)*. Therefore, a piezoelectric element can generate both charge and potential difference. All ferroelectrics have a well-defined polarization axis defined by the poling direction, which undergoes a change as the result of applied stress or electric field while in case of non-ferroelectric piezoelectric such as ZnO the polarization axis is defined by the crystal orientation. The polar axis is denoted by direction '3'. The in-plane directions at right angle to the polar axis could be considered same and marked as '1'. In most commonly used piezoelectric device configurations the stress is applied either parallel (d_{33} mode) or perpendicular (d_{31} mode) to the polar axis, as shown in Figure 5.[18] The maximum energy obtained from a piezoelectric element per cycle can be expressed as $\frac{c}{ab} d_{33} g_{33} F^2$ (for *33* mode) and $\frac{1}{a} d_{31} g_{31} F^2$ (for *31* mode). Here, d_{33} and d_{31} are piezoelectric charge coefficients (charge per unit force) while g_{33} and g_{31} are piezoelectric voltage coefficients (electric field per unit stress) in *33* and *31* directions respectively. These two configurations cover the most scenarios for practical piezoelectric energy harvesters. In addition, shear modes *(*such as d_{15}*)* have also been explored[94] and should be noted that there exist several other configurations which becomes more complex in the systems with lower symmetry.

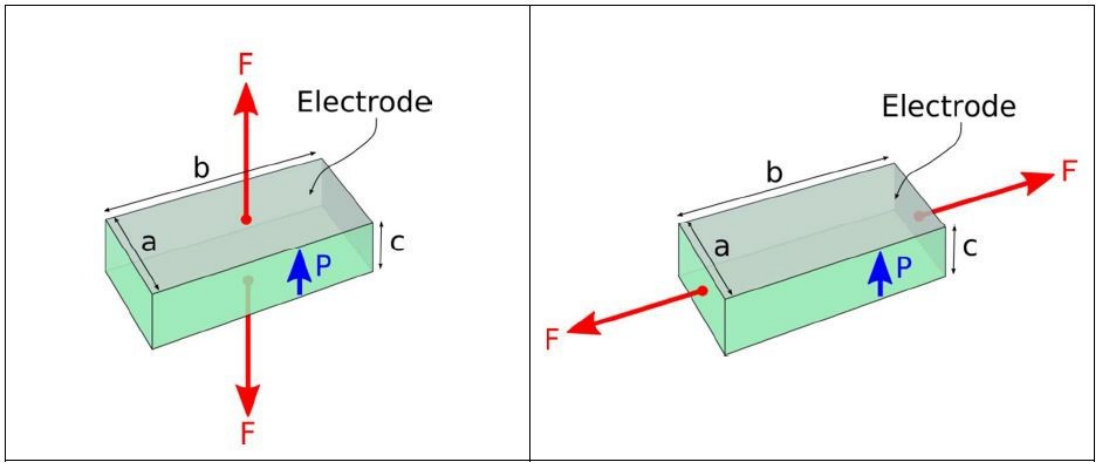

Figure 5: Schematic of (a) *33* and (b) *31* piezoelectric generator modes. Reproduced from reference[18].

3.3. Depolarization field

Ferroelectric materials possess a spontaneous polarization, i.e. electric dipoles are formed within the material. Ideally, if the ferroelectric is sandwiched between electrodes with the same work-function then the built-in voltage due to the presence of dipoles must be balanced by the presence of charges at the electrodes. However, in practice the free charges at the electrodes are not able to completely cancel the space and polarization charges which gives rise to internal fields in the opposite direction of polarization[95]. The cumulative internal field developed by these unscreened charges accumulated at the ferroelectric-metal interface is known as a *depolarization field* [58, 96]. It has been shown that the depolarization field is capable of changing the overall magnitude of the polarization, transition temperature, coercive field and the order of the phase transitions[97, 98], which can further affect the charge transport characteristics[99]. The presence of a finite electric field has the effect of separating carriers of opposite charge. In terms of device performance, this leads to improved carrier lifetimes, as the oppositely charge carrier are less likely to encounter and recombine. This concept was postulated early in halide perovskite research as 'ferroelectric highways' along which carriers could travel through the absorber layer.[100] It was subsequently shown, using simple Monte

Carlo simulations, that a degree of domain order exists in halide perovskites, even at room temperature.[86] Although visual inspection appears to show random disorder, an order parameter analysis reveals the presence of correlation between cation orientations. Early experimental work using piezoresponse force microscopy revealed the domain structure predicted by theory,[101] although full confirmation of domain structure and ferroelectricity in hybrid halide perovskites has proven more difficult and controversial.

4. Application in solar cells

Conventional solar cells are based on a *p-n* junction architecture[102]. A silicon *p-n* junction solar cell produces power by absorbing light to generate electron-hole pairs followed by the separation of charge carriers by the *p-n* junction and the collection of the electrons (in the *n*-type material as the majority carrier) and holes (in the *p*-type material as the majority carrier) by the electrodes. Figure 6 demonstrates the working principle of a simple *p-n* junction solar cell. The power conversion efficiency (η) of these cells is expressed as the ratio of output electrical power (P_{out}) to the input solar energy (P_{in}) absorbed. From the short circuit, current density (J_{sc}) and the open circuit voltage (V_{oc}), the efficiency can be calculated[103, 104]:

$$\eta = \frac{P_{out}}{P_{in}} = \frac{J_{sc} V_{oc} FF}{P_{in}};\ \mathrm{FF} = \frac{P_{out}}{J_{sc} V_{oc}} \tag{3}$$

where, FF is the *fill factor* and is defined as the ratio of the maximum obtainable power to the product of short circuit current density (J_{sc}) and the open circuit voltage (V_{oc}) and is limited by parasitic losses such as carrier recombination at the surface and within the bulk, series and shunt resistances. The timeline for the development of solar cells can generally be distinguished by the first, second and third generation of solar cells. Perovskite solar cells fall under the category of third-generation solar cells. Third generation solar cells employ more state-of-the-art concepts and materials including those that utilize electrostatically bound electrons and holes known as *excitons.* In contrast to the directly generated electron-hole pairs

in conventional *p-n* junction solar cells the excitons in such materials have low binding energy and hence induce more current by utilizing photons with comparatively less energy[105].

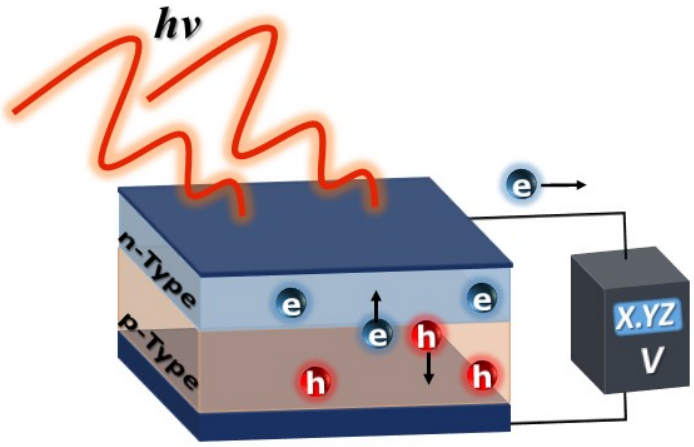

Figure 6: Working principle of a basic *p-n* junction solar cell.

4.1. Hybrid halide perovskite solar cells

Hybrid halide perovskites solar cells were first fabricated in the same manner as dye Sensitized Solar Cells (DSSCs) and gained popularity as a potential low-cost photovoltaic alternative[1, 3, 106]. The materials for DSSCs cells typically consist of wide band gap mesoporous semiconductors of high surface area, such as TiO_2, ZnO or SnO_2, which are sensitized with a nano-crystalline dye and anchored within a hole-conducting electrolyte or within a hole-transport material (HTM). The system is then sandwiched between two electrodes, one of which is transparent, which is further encapsulated with a glass layer. On exposure to sunlight, the dye absorbs light and a photoexcited electron transfers to the conduction band of the semiconductor and is finally carried to one of the electrodes[107]. Although initial hybrid halide perovskite solar cells were fabricated and thought to be operating analoguous to DSSCs, later studies revealed that hybrid halide perovskite solar cells work in a rather different way. It was shown that a single perovskite layer can be used for

both light absorption and electron-hole transportation.[108] In addition, unlike the common oxide based perovskites, which are categorized as third-generation solar cells, hybrid halide perovskites possesses a small binding energy similar to common inorganic materials such as Si and GaAs.[109-111] Therefore, it is now generally accepted that the hybrid halide perovskite solar cells operate as conventional *p-n* junction solar cells, similar to Si and GaAs. In hybrid halide perovskite solar cells, the perovskite absorber is sandwiched between a hole transport material (HTM) and an electron transport material (ETM). Inorganic TiO_2 or SnO_2 are commonly used as an ETM and organic or polymer HTM such as Spiro-OMeTED or PTAA are frequently employed for higher efficiency perovskite solar cells.[112-114] The operating principle and *p-n* junction profile has been effectively studied by electric potential profiling cross-section of the perovskite solar cells using Kelvin probe force microscopy (KPFM).[115, 116] A schematic of a cross-section KPFM measurement is shown in Figure 7 (a) and (b) and the cross-section of the device is prepared by either a focused ion beam or sample cleaving. To accurately determine the position of the junction, an external dc bias is applied, or light is illuminated on the device during the measurement. Figure 7 (c) to (f) shows results on profiles of the electrical potential and field and layer structure of the device consists of mesoporous TiO_2 layer and compact TiO_2. In this study, a *p–n* junction is found to be located at the TiO_2/perovskite interface for a planar type and the carrier concentration in the perovskite layer is roughly estimated to be 10^{16}-10^{17} cm^3, using a depletion width of 300 nm. For a mesoporous type, there is an n-p^- junction at the TiO_2/mesoporous interface, a weakly doped p^- mesoporous layer and a p^-/p potential barrier at the mesoporous/capping interface. The p^-/p potential barrier at the mesoporous/capping interface can prevent minority carrier (electrons), and thus improve the carrier collection.

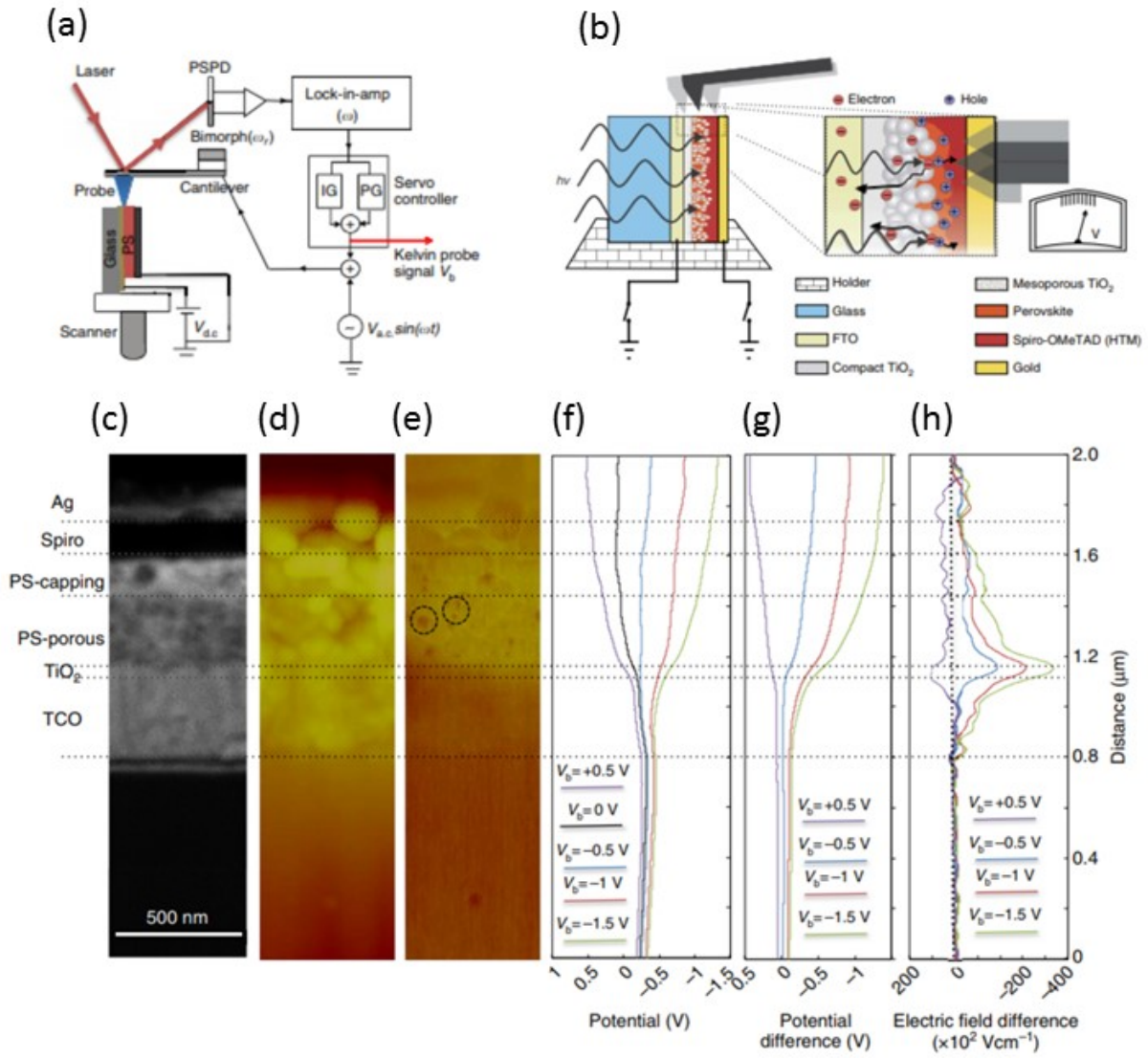

Figure 7: (a) and (b) Cross-sectional KPFM setup for contact potential difference (CPD) profiling. (c) SEM image; (d) AFM and (e) the corresponding KPFM images taken on the cross-section of the 280-nm porous device. (f) Potential profiles under the various V_bs. (g) Potential differences between those with the various V_bs and that with V_b=0. (h) Changes in the electric field by V_bs. The layer positions are indicated on the left of the figure, which are identified from the SEM image. The electric field covers the TiO_2/porous interface and the porous and capping layers, with the maximum at the TiO_2/porous interface. Example potential features such as the dark spots indicated by the dashed circles in (e) are caused by charges trapped on the cross-sectional surface. Reproduced with permission from references[115, 116]

Although hybrid halide perovskites are being investigated extensively, they still have technical barriers in terms of poor stability and the toxicity of lead for commercial deployment[117, 118]. In this context, Giustino and Snaith have provided an insight on various possible lead-free alternatives, which are shown in Table 1 of reference[6]. However, the continued investigation and search for improved materials is warranted as the efficiency achieved using lead-free counterparts remains relatively low. Recently, Wang *et. al.* reported a potential restriction on further progress in iodide based perovskite cells[119]. They revealed that iodide based perovskites produced gaseous iodine (I_2) during operation, which has a high vapor pressure and therefore permeates through the perovskite layer and results in degradation of the material[119]. Although they did not completely rule out the possibility of using iodide perovskites for solar cells, there is a need to develop new stable perovskites. Recently, Shin *et. al.* employed an inorganic perovskite ($MAPbI_3$), La doped $BaSnO_3$, as an electron transport layer to replace conventional TiO_2 and achieved a remarkable efficiency of 21.2% and photostability[120]. It retains 93% of its initial performance after 1,000 hours of exposure to sunlight.[120]

In addition, research is ongoing to understand the existence and possibility of ferroelectricity[121-124] in such materials and has also become a question of debate [86, 125-128]. A variety of potential mechanisms, as explained in section 2.3, with regard to the origin of ferroelectricity in both hybrid and inorganic perovskites have recently helped in identifying several hybrid halide perovskites which are ferroelectric in nature. One of the problems associated with hybrid halide perovskites is that ferroelectricity can be difficult to distinguish from several other effects.[129] Generally, one can test for ferroelectricity using the following approaches:

(i) Plotting of polarization *(P)* versus electric field *(E)* curves: Initial attempts to study *P* vs *E* curves for halide perovskites revealed no ferroelectricity, in contrast to theoretical predictions.[125, 130] However, interpretation of *P* vs *E* curves for halide perovskites

cannot be performed in the same way as for standard insulating ferroelectrics. It has been shown that the imaginary (lossy) part of the dielectric function needs to be studied as well as the real (storage) part, thereby characteristic *P-E* ferroelectric behavior can be observed in hybrid halide perovskites.[89]

(ii) Piezoresponse force microscopy (PFM): It can be used, but is difficult to interpret unambiguously due to presence of ionic movements.[101] However, recently there has been a demonstration of piezoelectricity in $MAPI_3$ that could be switched by an electric field. Moreover this study showed that light polarization is important for the ferroelectricity.[131] Another recent study has applied PFM showing differential charge extraction based on domain orientation,[132] strongly indicating the existence of ferroelectric domains. In addition, the presence of ferroelastic domains has been reported in $MAPI_3$ which can be modulated by applied stress (See Figure 8 (a)-(f)). It has been recently demonstrated that the chemical segregation and elastic vibration effects could be misguided as the presence of ferroelectricity.[71] Figure 8 (g)-(i) shows that on exposure to a laser source, variation in chemical mapping leads to formation of ferro-elastic domains.[71]

(iii) Second Harmonic Generation (SHG): Further evidence for ferroelectricity can be provided by the demonstration of second harmonic generation.[89] SHG can only occur in materials lacking inversion symmetry, therefore is a necessary but not sufficient condition for proving the existence of ferroelectricity.[88]

In summary, although the presence or absence of ferroelectricity in hybrid perovskites remains a controversial topic, a questions also remain as to the significance of ferroelectricity, ferroelasticity[71, 129] and stress induced domain switching[129, 133-135] or light induced changes in chemical mapping/ion migration[71] in determining the extraordinary performance of hybrid perovskite solar cells. Several convincing models for the possible beneficial effects of

ferroelectricity in these materials have been proposed and it is hard to ignore the potential benefits of having a functioning ferroelectric solar absorber layer. It is also interesting to note that inorganic perovskites with a ferroelectric nature are also being explored for photovoltaics and the effect is known as photo-ferroelectric/photoferroic or ferroelectric photovoltaic effect[37-43, 46, 50, 59, 136-146].

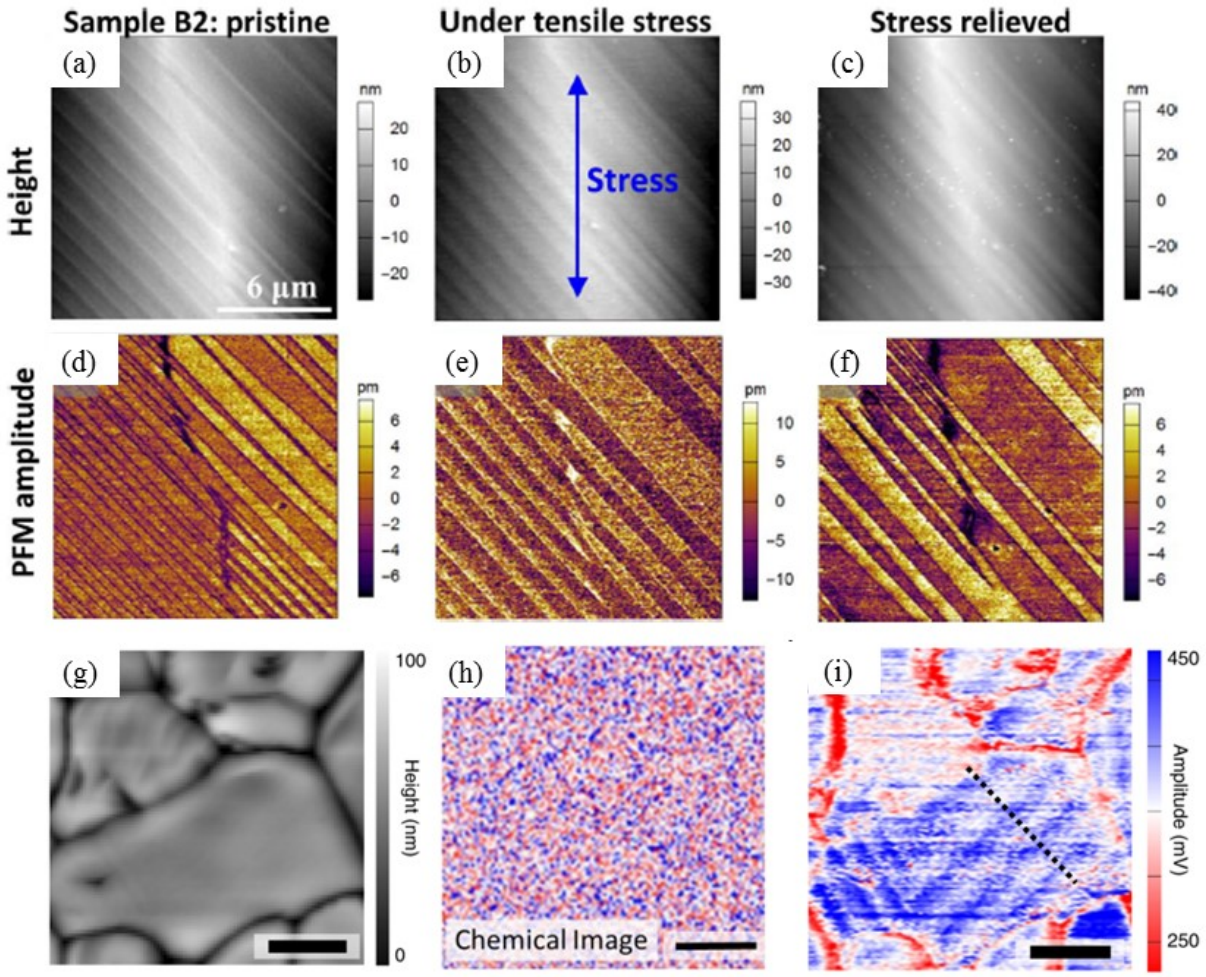

Figure 8: (a)-(f) Stress induced modulation of ferro-elastic domains in $CH_3NH_3PbI_3$ (reproduced from reference[129]). Light induced variation in chemical mapping (g) topography, chemical map (h) when laser is turned off and (i) when irradiated under a laser source of 1400 cm^{-1} under. Dashed line in (i) shows formed ferro-elastic domains (reproduced with permission from reference[71])

4.2. Ferroelectric perovskite solar cells

The dipole moment in ferroelectrics could be triggered by light induced localized heating, a fluctuation in internal field and interface band bending. This facilitates the generation and separation of charge carriers at the material-electrode interface. In the early 1970s, a *bulk* or *anomalous photoferroic/photovoltaic* effect was discovered in non-centrosymmetric crystals; this is also known as the *galvanic effect* or *non-linear photonics*[40, 48]. This effect in ferroelectric and multi-ferroic materials refers to the phenomena of obtaining a steady state current in the short circuit condition or a high output photovoltage in the open circuit condition in the direction of polarization of the materials on exposure to continuous illumination[39, 44]. Initial investigations focused on bulk materials, but it was later observed and studied at the nanoscale, which became a reason for the effect to be described as a '*bulk*' photovoltaic effect (BPVE); while the term '*anomalous*' photovoltaic effect (APVE) was used due to experimental observations of photovoltages 10^3 to 10^4 times higher at open circuit in contrast to the band gap of the material[39, 43]. Not all ferroelectrics exhibit an APVE, as it is dependent on the polarization magnitude[147], direction of polarization[38, 45, 148], light intensity[149], electrode spacing[150, 151], electrical conductivity[43] and the crystallography of the material[150, 152, 153], in addition to the nature of domain walls[37, 38] and material/electrode interfaces[140]. Its dependence on so many factors often leads to difficulty in reproducing the APVE, even in the same material[59, 138]. Therefore, several models have been proposed to explain the distinct type and nature of photoferroic effects. These include Schottky-junction effects, depolarization field effects and interface and domain wall effects[37, 38], which are now described below.

4.2.1. Bulk photovoltaic effect (BPVE)

The first model of BPVE was proposed by Glass *et. al.*[154] which was based on the asymmetry in materials. In recent years, Rappe and co-workers have developed theories based on shift currents.[155-159] Consequently, BPVE and APVE could now be explained at the

microscopic level using *ballistic* and *shift* mechanism models[44, 46]. The *ballistic model* for isotropic and anisotrpic materials in centrosymmetric (in the general case for *p-n* junction solar cells) and non-centrosymmetric crystals (in the general case for ferroelectric solar cells and asymmetric hybrid perovskite solar cells) is explained using Figure 9 (a) and (b), respectively[47]. This manifests itself that on exposure to an appropriate illumination the thermalized/hot carrier from the valence band is excited to the conduction band, thereby leading to the generation of a photocurrent. However, the presence of asymmetry or non-centrosymmetry in a crystal leads to a disparity in the momentum distribution of the carriers in the conduction band. The carrier then loses its energy and settles at the bottom of the conduction band by undergoing a band-band transition or a shift by distance l_o so as to equilibrate the asymmetric momentum and hence generating an additional photocurrent leading to BPVE[46, 47].

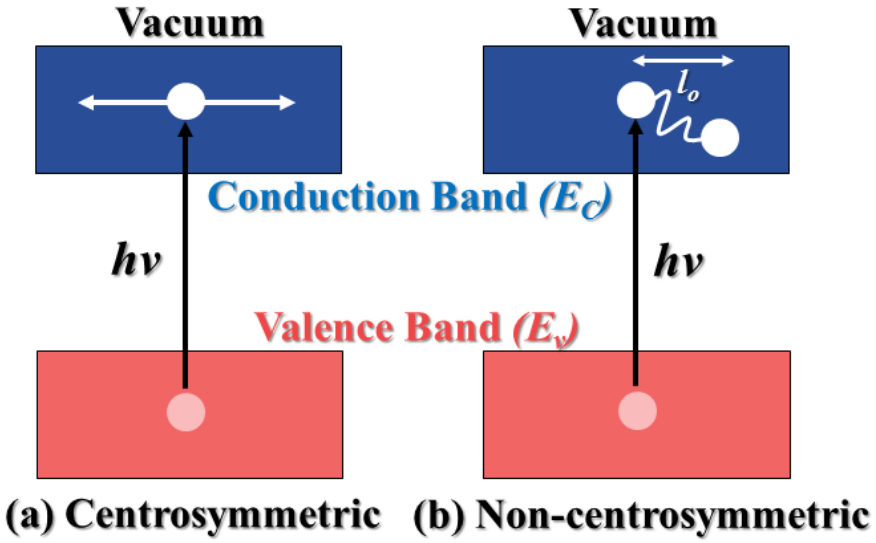

Figure 9: (a) Isotropic and (b) anisotropic non-equilibrium carriers' momentum distribution in centrosymmetric (general case for p-n junction solar cells) and non-centrosymmetric (general case for ferroelectric solar cells and asymmetric hybrid perovskite solar cells) corresponding to the classical and bulk photovoltaic effects, respectively. Adapted from references[44, 47]

In contrast, the *shift current* mechanism has a quantum-mechanical nature and the behavior of the thermalized carriers is governed by coherent excitations, rather than inelastic scattering, which allows for the net current flow from the asymmetry of the potential[155, 159, 160]. The same mechanism is also supported by experimentally verified first principle studies on $BaTiO_3$ and $PbTiO_3$ ferroelectrics[155, 156], multiferroic $BiFeO_3$ [156]and hybrid halide perovskites $CH_3NH_3PbI_3$ and $CH_3NH_3PbI_{3-x}Clx$ [157]. It is also suggested that the material itself can act as a current source[97,101,104] and the effect is also dependent on electronic structure and bonding interactions[155]. The total photocurrent (J) of a ferroelectric material in the closed-circuit condition can be given as the sum of steady current density (J_{sc}) generated due to illumination and the contribution of dark- (σ_d) and photo- (σ_{ph}) conductivities:

$$J = J_{sc} + (\sigma_d + \sigma_{ph})E \quad \text{or} \quad J = J_{sc} + (\sigma_d + \sigma_{ph})\frac{V}{d} \tag{4}$$

where E is the internal electric field developed between electrodes separated by distance d, and V is the applied voltage. In the open circuit condition, the total current (J) will vanish and hence the open circuit voltage (V_{oc}) is given as:

$$V_{oc} = \frac{J_{sc}d}{(\sigma_d + \sigma_{ph})} \tag{5}$$

The above expression suggests that V_{oc} will be anomalous if illumination leads to a significant rise in steady current density (J_{sc}). In addition, it is to be noted that the photoconductivity (σ_{ph}) is also dependent on light intensity[46, 48, 154, 161-163]. If the rise in σ_{ph} during illumination is of the order of the rise in $J_{sc,}$ then it will cancel out the influence of a rise in J_{sc} and cause the material to exhibit a constant or linear photoferroic effect. However, if there is a condition where $J_{sc}>>\sigma_{ph}>>\sigma_d$ then the effect will be 'anomalous' since V_{oc} in this case will increase abruptly. In addition, if $\sigma_{ph}+\sigma_d$ is insensitive to the light intensity, or the change in σ_{ph} is small in comparison to the magnitude of $\sigma_{d,}$ then this condition will also contribute towards the BPVE/APVE. In general, for most of the ferroelectric materials the case of $J_{sc}>>\sigma_{ph}>>\sigma_d$

exists and hence the V_{oc} for BPVE can be simplified to $\sim J_{sc}/\sigma_{ph}$. This can be further explained by substituting the following (μ: mobility of non-equilibrium charge carrier; α: absorption coefficient; τ: life time of non-equilibrium charge carrier; ξ: measure of exciton; l_0: mean free path; asymmetry; hv: photon energy; φ: quantum yield; q: positive elementary charge; Δn: excess charge carrier concentration; ϕ_0: photon flux density)[47, 96]:

$$J_{sc}=ql_0\xi\varphi\alpha \tag{6}$$

$$\sigma_{ph}=q(\mu_n+\mu_{ph})\Delta n= q(\mu_n+\mu_{ph})\varphi\alpha\tau\phi_0 \tag{7}$$

Hence, the efficiency of the BPVE/APVE can be expressed as[47, 96]:

$$\eta = \frac{J_{sc}^2}{\alpha I \sigma_{ph}} = \frac{J_{sc}^2}{\alpha I_0 (\mu\tau)_{ph}} \quad \text{or} = \frac{q\alpha\varphi(l_0\xi)^2 d}{4(\mu_n+\mu_p)\tau h\nu} \text{ with an assumed FF of 25\%} \tag{8}$$

Recently, a quantitative analysis by Fregoso *et. al.* established a relationship between polarization and magnitude of the shift current for *2-D* materials[164] and suggested that *2-D* ferroelectrics, such as GeS, will be ideal candidates for shift current photovoltaics (personal communication with Benjamin M. Fregoso).

Interestingly, the BPVE/APVE were first explained in ferroelectrics using the ballistic and shift current models. However, the first evidence of the BPVE/APVE effect was reported in paraelectric $BaTiO_3$[165], non-ferroelectric cadmium telluride[166-168] and zinc sulfide thin films[169]. It was suggested that this is due to the formation of surface space-charge layers[165] or stacking faults that produced a cumulative internal depolarization field[169]. Simultaneously, the same reasons were also thought to affect the process of domain nucleation[165].

4.2.2. Depolarization field driven ferroelectric photovoltaic effect

Interestingly, the polarization field is dependent on the material as well as electrode thickness and the area of contact[97, 98]. The depolarization field is negligible for a large inter-electrode distance in bulk ferroelectrics but is likely to increase with a reduction in inter-electrode

distance, as in thin films[95, 97, 98, 150]. This eventually makes it a governing factor for a number of applications in thin films as they significantly influence both the screening of spontaneous polarization and the separation charge carriers[145, 170-172]. In this context, Pintilie and Alexe postulated that the polarization bound charge is not located at the electrode but is slightly away at an atomic distance δ from the electrode and hence results in the formation of surface dipole layers that lead to a modification in the surface injection barriers[173]. Furthermore, this built-in voltage (V_{bi}) due to the difference in work function of the electrodes is modified by the surface dipole layers and is given as[96]:

$$V'_{bi} = V_{bi} + \frac{P_s \delta}{\varepsilon_0 \varepsilon_r} \tag{9}$$

The depolarization field for a metal contact with different dielectric constants (ε_{e1} and ε_{e2}) and screening lengths (l_{s1} and l_{s2}) for a dielectric constant (ε_F) can be written as[174, 175]:

$$F_{dp} = \frac{P}{\varepsilon_0 \varepsilon_F} \frac{\left(\frac{l_{s1}}{\varepsilon_{e1}} + \frac{l_{s2}}{\varepsilon_{e2}} \right)}{\left(\frac{l_{s1}}{\varepsilon_{e1}} + \frac{l_{s2}}{\varepsilon_{e2}} \right) + d} \tag{10}$$

The impact of the depolarization field on photovoltaic performance of thin films has been verified in several reports and it is believed that ultra-high thin films (10-50 nanometers) with high dielectric constant electrodes can aid in achieving high photovoltaic efficiencies[95, 97, 98, 150, 152, 170-172, 176-179]. Furthermore, it has been illustrated that it is possible to control the transport characteristics by controlling the direction of polarization[99]. The control over transport characteristics is also related to the Schottky barrier, which is another important mechanism for ferroelectric photovoltaics and will be discussed in the next section.

4.2.3. Ferroelectric Schottky-Junction effect

A Schottky barrier is formed at a ferroelectric-metal electrode interface due to the difference in work-functions, which leads to the development of a local electric field. On illumination, this built-in field drives the photocurrents by band bending at the interface[180]. Therefore, the barrier height and the depth of the depletion region plays an important role in the generation of photovoltages[180]; which is constrained by the material band-gap and work-function of the electrode [58, 59, 96]. As a result, the effect is probably less well studied in contrast to the bulk photovoltaic effect (BPVE). The overall barrier height can be enhanced by sandwiching a ferroelectric semiconductor between electrodes of different materials with a large difference in work function[49, 99, 140, 181-187]. This was first demonstrated by Blom *et. al.* in 1994[188] who sandwiched a ferroelectric $PbTiO_3$ film between a Schottky contact (Au) and an Ohmic bottom electrode ($La_{0.5}Sr_{0.5}CoO_3$) and showed that the Schottky barrier can be reduced by switching the polarization in the direction of the ferroelectric polarization. Another popular mechanism to tune the barrier height and width of the depletion region is to tune charged defects[183, 189]. In this context, the most common defect, namely vacancies, have been studied in hybrid halide perovskites[190, 191] and ferroelectrics[140, 189]. However, the photovoltaic effect obtained using this mechanism is not stable as the poled state of vacancies usually becomes unstable on removal of the electric field over time. However, it remains useful in distinguishing between the depolarization and Schottky junction based photovoltaic mechanism as it is possible to have switchable diode-like rectifying behavior using the Schottky junction effect[183, 186, 188] but not with the depolarization field[140]. Interestingly, the Schottky junction effect is independent of the direction of polarization and, therefore, it can be used to distinguish it from BPVE[192]. The understanding developed to date can aid in tuning the Schottky junction effect to support BPVE and achieve a combined photovoltaic response.

4.2.4. Interface and domain wall effects

Domain walls in complex oxides have been the focus of intense research over recent years. The fact that domain walls can be electrically conducting opens new pathways for a number of applications.[143, 193-196] Recently anomalous photovoltaic effects related to domain walls in ferroelectric materials have been reported.[37, 194, 197-203] Interestingly, electric-field control over the domain structure of a material allows the photovoltaic effect to be reversed in polarity or even to be turned off. The band structure and local bandgap of domain walls in ferroelectrics have also been studied.[204-207] In addition, photo-induced electrochemical effects at domain walls are a further interesting route in applications in water splitting[208] or for domain wall decoration (see[209] and references therein).

The spatial and temporal evolution of photoinduced charge generation and carrier separation in heteroepitaxial $BiFeO_3$ thin films was measured using Kelvin probe and piezoresponse force microscopy.[210] Contributions from the self-poled and ferroelectric polarization charge were identified from the time evolution of the correlated surface potential and ferroelectric polarization in both, films as-grown and after poling, and at different stages and intensities of optical illumination. Variations in the surface potential with bias voltage, switching history, and illumination intensity were investigated. It was shown that both bulk ferroelectric photovoltaic and the domain wall offset potential mechanisms contribute to the photo-generated charge. Polycrystalline[170], 2-D interfaces[211-214] and 1-D ferroelectric nanostructures have also been explored for enhanced photovoltaic responses[215, 216], in addition to nanoscale enhancements of ferroelectric photovoltaic effects at metal nano-tips.[141]

4.2.5. Summary of Ferroelectric Photovoltaic Effect

The photovoltaic performance of selected ferroelectrics is summarised in Table 1. Despite its 40 years of study, there remains much to be learned before a ferroelectric photovoltaic device

reaches any applications market. Although it is understood that non-centrosymmetry and polarization plays a crucial role in the bulk and depolarization field driven photovoltaic effect, the dynamics of the process remains unclear. The understanding of how ferroelectricity helps to achieve an enhanced photo-response is an open question[187]. Moreover, from the photovoltaics view-point, there is a strong requirement of developing new ferroelectrics with a narrow bandgap and improved conductivity. As a result, domain wall engineering and a controlled polarization can aid in raising the photovoltaic efficiency. In addition, there is a need to systematically understand charge carrier dynamics, such as mobility and diffusion length. Beyond this, other important considerations are the presence of piezo- and pyro-electricity in ferroelectrics as these effects along with photovoltaic effect can help in achieving a higher electrical output. One such attempt have been made by Rappe and co-workers where they tuned the band gap of a ferroelectric oxide to 1.1-1.38 eV.[50] Inspired by this, Yang *et. al.* recently illustrated an enhanced electrical output by simultaneously employing the pyroelectric and photovoltaic effect in lead-free ceramics.[49] The enhanced electrical output was observed to be approximately the same as the sum of photo- and pyro-currents measured individually under similar conditions. However, this cumulative effect could potentially increase near the transition temprature due to structural transition assisted charge fluctuations. Wang *et. al.* made an analogous attempt on hybrid perovskites and realized that it is possible to tune both the structural and optical properties by applying a pressure on the material[217]. However, this requires a special arrangement, but the pyroelectric effect could be exploited in parallel to the photovoltaic effect to enhance the overall energy conversion. Therefore, it is vital to understand the other possible mechanisms in perovskites that can help in obtaining an enhanced energy conversion under the exposure of light and electric field.

Table 1: Photovoltaic performance of ferroelectric materials.

Material	**Fabrication Method**	**Photovoltage**		**Photocurrent**			**Efficiency**	**Working Mechanism**
		V_{oc} (V)	**L**	**I_{sc} (μA**	**Light**	**Light**	**P_{out}/P_{in}**	

			(μm)	cm^{-2})	Intensity ($mW\ cm^{-2}$)	Wavelength (nm)	(%)	
STO/NSTO/ Bi_2FeCrO_6/ITO[218]	PLD	0.79	-	11700	100	Sunlight	3.3 (Single layer) EQE	**BPVE**
		0.84	-	20600	100	Sunlight	8.8 (multi-layer) EQE	**BPVE**
Nb-STO/ $BiMnO_3$, $BiMn_2O_5$/ITO [219]	PLD	1.48	-	7030	100	Sunlight	4.2	**BPVE**
Pt/PLZT(3/52 /48)/ITO[151]	MOD	0.86	4	1700	150	-	-	**BPVE**
		~496	2400	~16.8				
$BaTiO_3$[44]	Sputtering, FIB, PLD	8	-	17	100-470	405	100(EQE)	**BPVE**
Pt/Bi_2FECrO_6 /Nb–$SrTiO_3$[220]	PLD, Sputtering	0.74	0.125	990	1.5	635	6.5	**BPVE**
Au/PLWZT(3 /52/48)/Au[185]	Solution Coating	7.0	25	-	1.11	365	-	**BPVE**
ITO/PZT(53/ 47)/ITO[171]	PLD	0.45	0.4	0.006	0.45	-	0.6	**SCE & BPVE**
Fe/BFO/LSM /$SrTiO_3$[161]	PLD, Epitaxial	0.21	-	48	20	W-light	-	**SCE & BPVE**
Mg/PLZT(3/5 3/48)/ITO[180]	HPC	8.34	300	3.25	100	Sunlight	-	**PE & BPVE**
Pt:Pd/BFO/Pt :Pd[141]	Mix-flux Technique	6 - 30	50-300	10^7-10^8	40,000	405	40(IQE)	**TE & BPVE**
Pt/PZT(20/80)/Pt[192]	Sputtering	-	0.36	~8	10	350-450	-	**SCE & BPVE**
Au/PLWZT(3 /52/48)/Au[182]	Sol-gel	0.6	0.706	-	0.74	365	-	**SCE**
Pt/PZT(52/48)/Pt or Ni[221]	Sol-gel	~0.8	0.2	~0.03	0.05	300-390	-	**SCE**
$SrRuO_3$/BFO/ ITO	MOCVD	0.8 - 0.9	0.2	1500	285	Sunlight	10 (EQE)	**SCE**
Au/BFO/Au[222]	Mix-flux Technique	~0.08	80	8.219	<20	532	-	**SCE**
$SrRuO_3$/BFO/ Au[223]	Sputtering, Epitaxial	0.286	0.17	0.4	750	435	-	**SCE**
Au/BFO/Au[183]	Mix-flux Technique	~0.7	60	1.58	20	532	1.5 (EQE)	**SCE**
Nb-doped $SrTiO_3$/BFO/ Au[224]	PLD	~0.15	0.1	6000	285	W-light	0.03	**SCE**
ITO/PZT/Cu_2 O/Pt[225]	Sol-gel	0.6	270	4800	100	Sunlight	0.57	**SCE**
Pt/Poly-BFO/Au & ITO[170]	Sol-gel	0.1	0.3	~1	450	340	-	**SCE & DF**
Graphene/Poly-BFO/Pt[226]	Sol-gel	0.20	0.3	2800	100	Sunlight	-	**MIM-SCE**

Nb: $SrTiO_3$/PLZT (3/52/48)/LSM[145]	Sputtering, Epitaxial	~0.7	0.068	~0.8	0.059	-	0.28	**DF**
Pt/BFO/Pt[38]	MOCVD	16	200	120	285	W-light	10^{-3} (EQE)	**DW**
Pt/BFO/Pt[37]	MOCVD	0.014	One DW	50	100	W-light	10(IQE)	**DW**
FTO/Poly-BFO/AZO[172]	CSD	0.63	-	130	100	Sunlight	7 (EQE)	**BI & DF**
ZnO : Al/BFO/LSC[227]	PLD	0.22	0.35	~5	1	W-light	-	**-**
Ag/Pr-doped BFO NTs/Ag[215]	Chemical Technique	0.21	-	-	10	Sunlight	~0.5	**-**

BPVE=bulk photovoltaic effect; DF=depolarization field effect; SCE=Schottky contact effect; DW=domain wall effect; MIM=metal/insulator/metal junction, PE=photoelectric effect; BI=built-in potential due to asymmetric electrodes; TE=tip enhancement effect; MOD=metal–organic decomposition; MOVCD=metal–organic vapor phase epitaxial; FIB=Focused ion beam milling; PLD=pulsed laser deposition; HPC=hot-pressing calcinations; CSD=chemical solution deposition; IQE=internal quantum efficiency; EQE= external quantum efficiency

5. Perovskites for thermoelectrics

5.1. Ferroelectric thermoelectrics

Thermoelectric generators are devices which convert temperature differences into electrical energy. The principal phenomenon which underpins this energy conversion are the Seebeck effect (i.e. the conversion of a thermal gradient into electricity) and Peltier effect (i.e. achieving a temperature gradient by passing a current through two junctions).[228-230] The thermoelectric effect have been widely employed for scavenging of waste thermal energy and the efficiency of a material for thermoelectric application is measured by its figure of merit, zT: [51]

$$zT = S^2 \sigma T / \kappa \tag{11}$$

Where, S is the Seebeck coefficient and is defined as the ratio of the voltage change induced by a temperature change for a material with thermal and electrical conductivities κ and σ respectively. $S^2\sigma$ is termed the thermoelectric power factor. To achieve a high thermoelectric efficiency the material should have a high electronic charge carrier concentration ($\sim 10^{18}$ to $\sim 10^{21}$ cm^{-3}) and high electronic conductivity. An increase in carrier concentration will not only increase the electric conductivity but simultaneously enhance thermal conductivity

which results in a decrease of the *zT* value and reduced thermoelectric performance. In addition, the major roadblocks in the development of materials for this technology include a limited working temperature range, the use of toxic chemicals and high processing costs, while some materials such as chalcogenides and antimonides have issues of oxidation at high temperatures.[51] In the search of potential candidate materials which can overcome the above mentioned issues, oxygen-deficient ferroelectrics with high conductivities have provided a new direction.[231, 232] $SrTiO_3$ based materials have been well studied, but their *zT* values are limited to ~0.1 due to moderate thermal conductivities.[233-240] In addition, $CaMnO_3$-based systems have a high Seebeck coefficient, low thermal conductivity and tunable resistivity[241, 242], which are ideal properties for improved thermoelectric applications. Theoretical estimations suggests that it is possible to have *zT* values greater than one in $CaMnO_3$.[243] Lee *et. al.* reviewed future directions in ferroelectric based thermoelectricity and stressed the potential of obtaining a high thermoelectric effect in n-type perovskite $BaTiO_3$ and tungsten bronze $(Sr_{1-x}Ba_x)Nb_2O_{6-\delta}$ systems[51] and concluded that thermoelectric ferroelectrics with improved performance could be achieved by a better understanding of the mechanism behind the electronic interactions, defect states and oxygen vacancies. However, from a device perspective it is easy to optimize a pyroelectric (as it is easy to have time dependent temperature change rather than inducing a large thermal gradient over a ferroelectric thin film or bulk material) based system instead of a thermal gradient (thermoelectric effect) based system on ferroelectric materials.[30] Consequently, a maximum Carnot efficiency of only 1.7% was reported using the thermoelectric effect, while the same is found to be 50% for a pyroelectric device.[30]

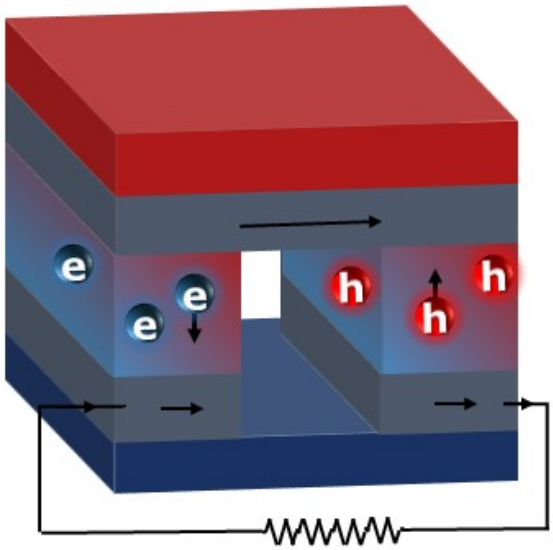

Figure 10: Schematic of a thermoelectric module showing the direction of charge carriers when operated between a hot (red) and cold (blue) temperature source.

5.2. Hybrid halide perovskites for thermoelectrics

In parallel research efforts on ferroelectric thermoelectrics, there exists a branch of organic thermoelectric materials which have recently gained significant interest among researchers because of their relatively low cost of manufacture, ease of fabrication and possibility of developing flexible thermoelectric modules[244, 245]. Table 2 provides an overview of thermoelectric performance estimates of selected hybrid halide perovskites. He and Galli conducted a pioneering first principle study of $CH_3NH_3AI_3$ (A=Pb and Sn) for thermoelectric applications and realized that it is possible to have a zT in the rage of 1 to 2 by engineering hybrid halide perovskite superlattices with carrier concentrations of the order of ~10^{18} cm^{-3}.[52] Their study suggests that these perovskites may possess a large carrier mobility due to small carrier effective masses and weak carrier-phonon interaction. These materials have a large Seebeck coefficient and low thermal conductivities, which makes them ideal candidates for thermoelectric energy harvesting. However, their electrical conductivity needs to be enhanced and this could be achieved by chemical or photoinduced doping.[246] Lee *et. al.* have used

Density Functional Theory to suggested that $CH_3NH_3AI_3$ has a poor thermoelectric performance but it can be increased to the levels of the existing best thermoelectric counterparts (Bi_2Te_3) by electron-doping.[247] The claim was further supported in a theoretical study by Filippetti *et. al.* where they reported the possibilities of achieving a room temperature thermoelectric effect with *zT* values ranging between 1 to 3.[248] Thereafter, Wang and Lin conducted Molecular Dynamics simulations and provided atomistic insights on ultralow phonon transport over a wide temperature range in these materials.[249] Recently, Zhao *et. al.* conducted a first principle study and suggested that hole-doping optimization could provide better thermoelectric performance over the electron-doped one.[250] In addition, they proposed to tailor the organic cation vacancies for better thermoelectric performance. By taking advantage of tuning the electrical conductivity by optimized doping, these studies postulate that hybrid halide perovskite more suitable for thermoelectric energy conversion in contrast to their ferroelectric counterparts. However, at this stage it is difficult to accurately predict the exact status of these materials as thermoelectric generators due to the lack of experimental confirmation. It is important to note that the thermoelectric effect utilizes a thermal gradient while there exists another mechanism (pyroelectric effect) which is based on a time dependent thermal fluctuation. Before understanding pyroelectric energy conversion, it is important to understand how perovskites can be used to store electrical energy, which are now discussed.

Table 2: Thermoelectric performance estimates of selected hybrid halide perovskites.

Material	**σ (Ω cm^{-1})**	**S (μV/K)**	**σS^2 (10^{-4} W/mK^2)**	**κ (W/mK)**	**ZT**	**Temperature (K)**	**type**
$MAPbI_3$[248]	160	-238	8.4	0.1	0.38 (SC) /0.61 (PC)	300	n-type
$MAPbI_3$[248]	94	181	3.1	0.06	0.15 (SC)/ 0.25 (PC)	300	p-type

$MAPbI_3$[248]	89	-362	10.5	0.145	1.06(SC)/ 1.61 (PC)	600	n-type
$MAPbI_3$[248]	41	295	3.6	0.06	0.43 (SC)/ 0.71(PC)	600	p-type
$MAPbI_3$[248]	68	-428	11.3	0.151	1.74 (SC)/2.56 (PC)	800	n-type
$MAPbI_3$[248]	25	358	3.3	0.04	0.64(SC)/ 1.08 (PC)	800	p-type
$MAPbI_3$[247]	62	800	40	1.2	2.27	400	n-type
$MASnI_3$[247]	27	1600	70	1.2	3.31	400	n-type
$FAPbI_3$[247]	62	800	30	1.2	1.18	400	n-type
$FASnI_3$[247]	19	1600	50	1.2	4.99	400	n-type
$MAPbI_3$[52]	-	-320	-	1	1.7	300	n-type
$MAPbI_3$[52]	-	380	-	1	1.1	300	p-type
$MASnI_3$[52]	-	-400	-	1	1.2	300	n-type
$MASnI_3$[52]	-	240	-	1	0.8	300	p-type

SC= Single crystal; PC= Polycrystalline

6. Perovskites for energy storage

6.1. Ferroelectric perovskites for capacitor applications

Ferroelectric materials and their composites have been studied in detail for ultra-high density capacitor applications.[251-264] The energy storage capcaity of a parallel plate capacitor can be determined as $C = \varepsilon_0 \varepsilon_r \frac{A}{d}$ (A= area of contact; d=thickness of a dielectric layer; ε_0= vacuum permittivity; ε_r= relative dielectric permittivity). In the case of ferroelectrics, an externally applied voltage (V=Ed; E= applied electric field due to voltage V) leads to an electric displacement (D= P + $\varepsilon_0 E$). D is assumed approximately equal to P in case of high dielectric

permittivity materials such as ferroelectrics, relaxors and anti-ferroelectrics. The maximum applied electric field is limited to the breakdown strength of the material. The stored (U_{Stored}) and recoverable (U_{Recov}) energy density of such materials is given as[259-265]:

$$U_{Stored} = \int_0^{P_s} EdP \quad (12)$$

$$U_{Recov} = \int_{P_r}^{P_s} EdP \quad (13)$$

The equations above suggests that the recoverable energy density of a ferroelectric capacitor is dependent on the magnitude of polarization, dielectric constant and the breakdown strength of the material. Interestingly, the dielectric constant and hence polarization are dependent on operating frequency, electric field and temperature. The dielectric constant of a ferroelectric is generally a cumulative effect of surface or interface charges, dipoles, ions and electronic contributions. Relaxation of these contributions govern the operating frequency and dielectric constant of the ferroelectrics. Prime research is focused on achieving a higher dielectric constant and breakdown strength. In this context, relaxor ferroelectrics, ferroelectric-polymer and ferroelectric-glass composites are being explored and have been proven as good alternatives[253-255]. The shaded area of Figure 11 illustrates the recoverable energy storage and clearly indicates that for high-energy storage, the material should have a low remnant polarization and high saturation polarization with a low hysteresis, as observed in the case of relaxor ferroelectrics (Figure 11 (b)). It is to be noted that in addition to these parameters the material should also possess low leakage current and dielectric losses.[253, 255-257] A more detailed discussion of the state-of-the-art progress can be found in a recent reviews[251, 259-262]

Although ferroelectrics have a proven potential as a dielectric material in a parallel plate capacitor structure, hybrid halide perovskites rather fit more for an electrode material because of their relatively high surface area, electronic conductivity and associated losses. Therefore, utilizing these two classes of perovskites together for this application is more promising rather than expecting utilization of a single material. In this way, the energy converted through

perovskite dielectric or electrode layer could be stored for a long time and will be ideal for next generation photo-capacitors (discussed in section 6.4). Hybrid halide perovskites have also been explored for an electrode or an electrolyte in supercapacitors.[266-268]

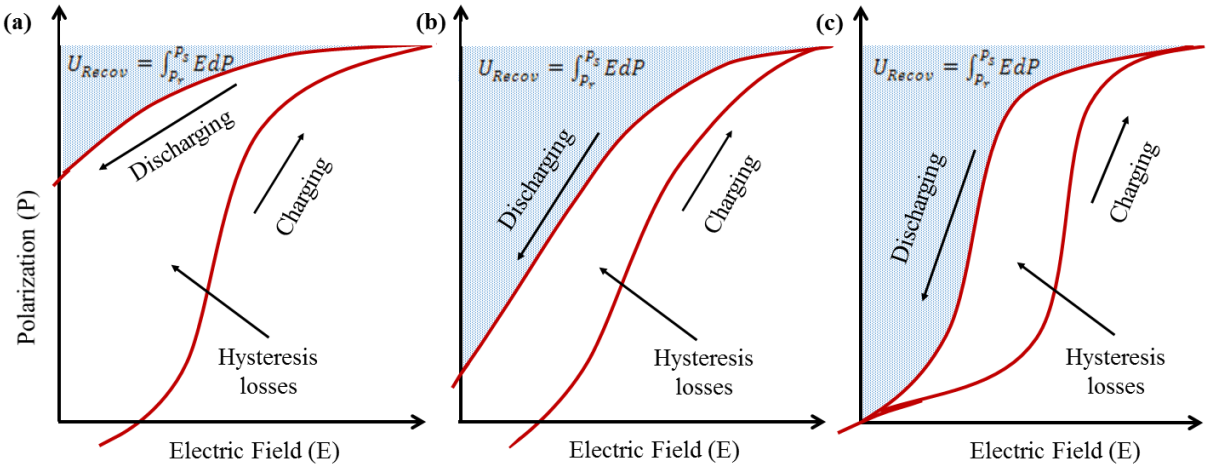

Figure 11: A schematic of energy density storage estimation (highlighted shaded area) from the Polarization–Electric field *(P-E)* behavior of (a) ferroelectric, (b) relaxor ferroelectric and (c) antiferroelectric materials. Adapted from references[251, 256, 263-265]

6.2. Hybrid halide perovskites for supercapacitors

Recently, Zhou *et. al.* reported a thin film electrochemical capacitor (5.89 μFcm^{-2}) based on an organo-lead-triiodide perovskite which exhibited a stable capacitance beyond 10^5 cycles[268]. Such an approach provides a novel dimension for studying the ionic properties of hybrid halide perovskites and developing new devices. The observed two electric double layer capacitances were attributed to ion migration at the perovskite/electrolyte and perovskite/FTO interfaces.[268] Shortly after, a perspective article by Snaith *et al.* postulated that the high surface area and ionic mobility of hybrid halide perovskites could make it a good alternative as an electrode or electrolyte in a supercapacitor.[266, 267] Afterwards, a capacitance of 5.5 mFcm^{-2} with a retention rate of beyond 10^4 cycles was reported using methylammonium bismuth iodide $(CH_3NH_3)_3Bi_2I_9$.[269] The major difference between a supercapacitor and a parallel plate capacitor is that the dielectric layer is replaced by an electrolyte in-between the

electrodes. The ions in the electrolyte respond to the electric field, in contrast to the dipoles in a dielectric. Although research in this area has only just begun (in 2016) the presence of ferroelectric/ferroelastic domain walls and diploes could enhance the performance of these capacitors in the same way as in the case of ferroelectric based parallel plate capacitors. It is to be noted that Zhou *et. al.* claimed that '*ion formation and transport processes in organometal halide perovskites are largely activated by free charge carriers and may also be interface-dependent*'.[268] Ion migration is found to be a plausible reason for the presence of ferroelastic domains in hybrid halide perovskites[71, 270] which could be further tuned by applied stress[129], applied electric field[270] and light intensity[270]. Theoretical estimates suggest that the presence of domain walls in hybrid halide perovskites are expected to facilitate band-bending and charge separation.[203] Therefore, accelerated ion formation and migration is likely to support charge separation in perovskite supercapacitors. The same reasons could also be helpful in utilizing these materials in battery applications, which will now be described.

6.3. Hybrid halide perovskites for batteries

Generally, solid state batteries are comprised of two lithium storing electrodes and an ion-conducting electrolyte. During charging, the lithium ions are driven into the anode by intercalation and the positive charge is compensated by the electrode.[271] During discharge, the Li-ions move back to the cathode and the current produced by the corresponding reverse flow of electrons is used to power the device.[272] In 2015, Xia *et. al* reported that $MAPbX_3$ (X=Br, I) is a potential anode material for lithium ion batteries with storage capacities of ~43.6 mAh g^{-1} ($MAPbI_3$) and ~331.8 mAh g^{-1} ($MAPbBr_3$).[273] While the storage capacity of a $MAPbBr_3$ based battery reduced to 175 mAh g^{-1} after 15 discharge cycles, it remained comparable to commercial $Li_4Ti_5O_{12}$ anode.[273] However, it was not clear if the Li-ion was stored by intercalation or if it was a surface phenomenon. Vicente and Belmonte further

explored the intercalation mechanism of $MAPbBr_3$ and Li ions, and confirmed the superionic nature of $MAPbBr_3$.[274] They found that Li^+ could exhibit a high diffusion rate (10^{-7} cm^2s^{-1}) within the perovskite lattice with small structural distortions, which could lead to conductivities of the order of 10^{-3} $\Omega^{-1}cm^{-1}$. Using this approach, they illustrated that outstanding capacities of ~200 mAh g^{-1} could be maintained with good reversibility. The same year, Tathavadekar *et. al.* reported capacities of 646 mA h g^{-1} and 315 mA h g^{-1} for Li- and Na-ion batteries using engineered low dimension hybrid halide perovskite (benzidine).[275] The device found to be stable for 250 cycles. In 2018, Ahmad *et. al.* utilized 2-D hybrid halide perovskites ($MAPbX_3$; X=Br, I) for simultaneous generation and storage of electrical energy.[276] These *"photo-batteries"* developed by Ahmad *et. al.* were reported to retain storage capacities of up to 100 mAh g^{-1}.[276] Ramirez *et. al.* further explored 3-D ($CH_3NH_3PbI_{3-x}Br_x$) and 2-D ($(CH_3NH_3)_2(CH_3(CH_2)_2NH_3)_2Pb_3Br_{10}$) mixed halides for battery applications and proposed that the lithium insertion-extraction mechanism is accompanied by alloying-dealloying of intermetallic Li_xPb.[277] It was found that bromide plays a crucial role in lithium intercalation and storage capacities of ~375 $mAhg^{-1}$ and ~500 $mAhg^{-1}$ were observed in $(CH_3NH_3)_2(CH_3(CH_2)_2NH_3)_2Pb_3Br_{10}$ and $CH_3NH_3PbBr_3$, respectively.[277] Recently, Wang et. al. demonstrated excellent cyclic stability (1000 cycles) in $CH_3NH_3PbBr_3$-based batteries.[278] Besides these achievements, rapid deterioration of the electrode is still a major obstruction in commercializing these materials in a battery. Further investigations in this direction revealed that post-poling ion migration is much faster at grain boundaries than within the grains[279], which supports the claim of the Xia *et. al.*[273] and has motivated researchers to develop novel perovskites to address the key challenges of achieving improved storage capacity and electrode stability at comparatively low cost, as compared to current commercially available batteries.

6.4. Photo-capacitor

A photo-capacitor is a self-charging device which not only converts solar energy into electrical but also stores the converted electrical energy. The concept was introduced by Miyasaka and Murakami in 2004[280] and is illustrated in Figure 12. They used a multilayered photoelectrode comprising of dye-sensitized semiconductor TiO_2 nanoparticles followed by a hole-trapping layer (LiI) and activated carbon particles in contact with an organic electrolyte solution. The key idea is to store the photogenerated carriers at the electric double layer so that the device can be self-charged on exposure to light. Miyasaka and Murakami's[280] device was found to yield charging voltages of >0.45 V and a capacitance of 0.69 Fcm^{-2}. Furthermore, with repeated cycles the reported coulombic efficiency was 80%. Since hybrid halide perovskites emerged as a replacement of the dye-sensitized solar cells therefore, these have also been explored for photo-capacitor application.[281, 282] Liu *et. al.*[281] used $MAPbI_3$ as an absorbing layer and achieved a capacitance of 0.422 Fcm^{-2} with high coulombic (96%) and energy storage (70.9%) efficiencies. In recent work, a $CsPbBr_{2.9}I_{0.1}$ perovskite-sensitized solar cell was integrated with an asymmetrical supercapacitor and a photo-capacitance of 0.030 Fcm^{-2} was achieved.[282] The energy storage capability of the supercapacitor when operated individually was found to be 0.15 Fcm^{-2} with only 4% losses over 1000 charge/discharge cycles. The photo-capacitance was low due to the cut-off potential of 0.07V. These observations help in concluding that hybrid halide based photo-capacitors have strong future potential but need to be explored more. Concurrently, the energy stored in ferroelectric capacitors is also found sensitive to light.[283, 284] A decrease in ferroelectric capacitance on exposure to light is obvious as the photogenerated carriers will induce leakage current. This phenomena is being explored for photosensors.[283, 284] However at the same time, there is a possibility of a light induced capacitance increase using appropriate device configuration[285]. Several reports suggest that the dielectric constant of some ferroelectrics is sensitive to light[286, 287] which puts them forward for photo-capacitor application. Intriguingly, a photo-capacitor based on ferroelectrics will have a simple device architecture (a parallel plate

capacitor with transparent electrodes) in contrast to hybrid halide perovskites because light could directly change the state of polarization in ferroelectrics. Apart from these attempts, the field is not much explored and may offer new possibilities in areas such as optoelectronic memories, diodes and sensors.

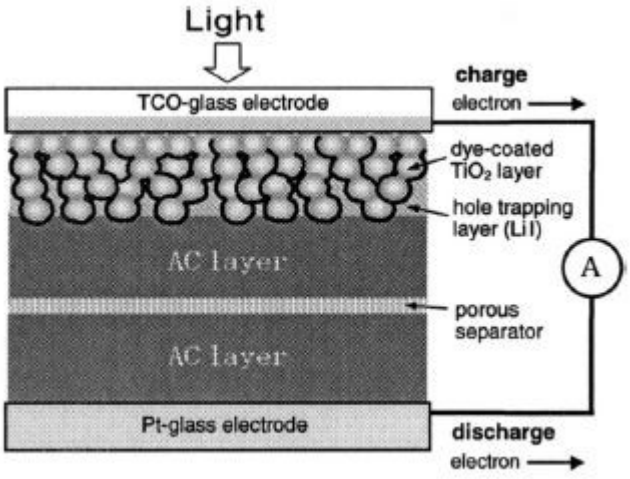

Figure 12: A schematic of a photo-capacitor designed by Miyasaka and Murakami. Reproduced from reference[280].

7. Piezo-electric and pyroelectric energy conversion using perovskites

Pyroelectric and piezoelectric materials can generate a potential difference when heated or stressed repectively and the generated potential difference could be utilised to obtain an electrical output through an external circuit. These both are necessary, but not sufficient, conditions for ferroelectricity. The debate on ferroelectricity, piezoelectricity and pyroelectricity in hybrid halide perovskites and their potential for these applications cannot be ignored.[89, 288, 289] Recently $MAPI_3$ was proven to be pyroelectric and the effect can be distinguished from the thermoelectric effect by applying a heat source to alternating sides of the crystal sample and observing the difference in thermally generated current in each direction.[89] Interestingly it has also been shown that $MAPbBr_3$ is *not* pyroelectric, and is therefore not ferroelectric.[88] However, the literature suggests that the poling direction of a

ferroelectric layer sandwiched in organic solar cells can help in charge collection and hence result in improved photovoltaic efficiency.[290] Similarly, attempts have been made to utilize hybrid halide perovskites together with well-known ferroelectric/piezoelectric/pyroelectric materials to attain better piezo- or pyro- outputs by taking advantage of excellent charge transport properties of hybrid halide perovskites.[291-293] Another possible way to utilize perovskites for an enhanced pyro- and piezo-electric output is cycling energy conversion. It has been suggested that the piezo- and pyro-electric short circuit current can be enhanced to several orders of magnitude by employing stress[15, 23, 25] or thermal[14, 17] energy conversion cycles. In this context, Mohammadi and Khodayari advocated for the use of an Ericsson cycle[294] knowing that there exist several other cycles based on the mode of operation[33, 36]. These include resistive cycles[33], synchronized electric charge extraction cycles[33, 36] and synchronized switch damping on inductor (SSDI) cycles. Details about these cycles can be found in reference[19]. It has been found that the *Olsen cycle* (for cyclic pyroelectric energy conversion) and its stress driven counterpart (for cyclic piezoelectric energy conversion), which are well-known variants of the Ericson cycle, perform well in this regime[295-297].

7.1. Cyclic energy conversion

The Olsen cycle operates under unipolar electric fields, rather than bipolar electric fields used in the conventional Ericson cycle, and therefore has a reduced hysteresis loss and enhanced energy conversion. The energy harvested using the Olsen cycle is not merely a contribution of the pyroelectric effect but also takes advantage of the electrical energy storage capacity of the material as a result of the change in capacitance (permittivity) of the material with temperature. For this reason, the cycle is claimed to be capable of providing an energy density of three orders in magnitude higher than that obtained using the conventional pyroelectric effect[20]. Olsen *et. al.* experimentally verified this claim for a number of well-known compositions[295-302] which has been supported by a number of studies [10-14, 20-22, 24, 303, 304].

This made the Olsen cycle the primary mechanism for pyroelectric energy harvesting. Since the cycle is based on a temperature dependent polarization behavior, it is important to note that, in general, the saturation polarization decreases with an increase in temperature and such a response is referred to as a 'thermal fluctuations-1 (TF-1)' behavior while the case where the saturation polarization increases with an increase in temperature, i.e. where the hysteresis loop tends to become linear at low temperatures rather than at high temperatures, is known as 'thermal fluctuations-2 (TF-2)' behavior[14, 17]. Since TF-2 compositions were rarely observed before 2008, the Olsen cycle was initially proposed for the commonly observed TF-1 ferroelectrics. In 2014, Vats *et. al.* proposed a modified version of the Olsen cycle for TF-2 compositions [14] and generalized it for materials that exhibit a change in polarization with temperature fluctuations[14, 17]. Figure 12 (a) and (b) show the working principle of an Olsen cycle for TF-1 and TF-2 composition, respectively.

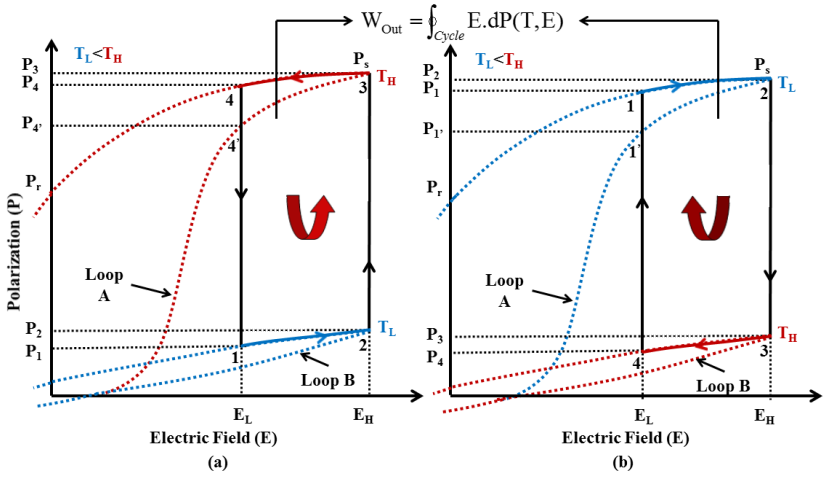

Figure 13: Working of an Olsen cycle for (a) TF-1 and (b) TF-2 compositions and the area covered by the loop 1-2-3-4 shows the harvested energy.

The modified cycle states that the material should initially be polarized under a unipolar applied electric field at the lower temperature *(T_L)* and then exposed to a heat source isoelectrically *(E_H)*. This leads to a polarization change (a decrease for TF-1 and increase for TF-2) that can be simultaneously converted into an electrical output. Subsequently, the material is depolarized under a unipolar applied electric field at a constant higher temperature

(T_H) followed by an isoelectric *(E_L)* cooling step. This provides an output electrical impulse in the form of harvested electrical energy. Figure 13 (a) and (b) provide a schematic explanation of a typical Olsen cycle for TF-1 and TF-2 materials, respectively. Further, the area enclosed *(1-2-3-4)* by the complete cycle on a corresponding *P-E* curve gives the net harvested output electrical energy density (N_D) per liter per unit cycle [21, 301]:

$$N_D = \oint E.\mathrm{d}P \tag{14}$$

It is important to note that for a material to work with a practical Olsen cycle, an arrangement is needed to achieve specialized oscillating heat currents and an external load circuit is required for receiving an electrical output. A variation in the design of such an arrangement can significantly influence the degree of harvested electrical energy density. It is to be noted that obtaining a change in polarization by applied stress instead of a temperature change could be operated in a similar fashion for cyclic piezoelectric energy conversion and the energy density can be estimated using equation 14.[15, 23, 25]

The energy conversion through Olsen cycle should be equally true for non-ferroelectric materials or materials with high thermal losses where a change in electrical properties, such as permittivity, is observed with thermal fluctuations or mechanical vibrations. In such a case, the temperature or stress dependent electrical response could be utilized in a cyclic fashion. However, the efficiency will be reduced due to significant non-recoverable input during the process of applying and removing electric field. In the case of hybrid halide perovskites, temperature dependent ion migration[305-307] will play a significant role in contrast to the dipoles, as in the case of ferroelectrics. Although there are no reports on cyclic energy harvesting using hybrid halide perovskites, probably due to the associated large dielectric losses, the possibility of obtaining an enhanced electrical output using such strategies is of interest especially when stress induced modulation of ferro-elastic domains in $CH_3NH_3PbI_3$[129] is already well known.

8. Future Prospects

The above discussion suggests that each technology and mechanism has its own desired characteristics, efficiency limit and corresponding advantages and disadvantages, such as a high band gap and low absorption coefficient restricts the photovoltaic performance in ferroelectrics, while technological constraints restrict single junction and silicon photovoltaics to 30% (Shockley and Queisser limit)[308]. Similarly, the ability to achieve a high thermoelectric operating temperature for ferroelectrics is an issue, while the absence of the desired electrical conductivity in hybrid perovskites is a barrier for thermoelectric applications. Consequently, there is a need to develop new materials with a suitable range of properties for effective utilization of available solar and thermal resources. In parallel, the approach of simultaneously engaging multiple energy conversion mechanisms could be envisaged[16, 309, 310]. Recently, a breakthrough in this direction is reported where the photovoltaic response of the material is significantly enhanced by simultaneously using light, thermal fluctuations and stress. Yang *et. al*. tuned the bandgap (~1.6 eV) of ferroelectric $(KNbO_3)_{1-x}$-$BNNO_x$ ceramics so as to have simultaneous advantage of pyroelectric and piezoelectric effect to achieve above-band gap photovoltages.[49, 311] Another illustration is reported by Zhang *et.al.*[180] who enlarged the photovoltaic response of a device by combining the classical photovoltaic effect with the ferroelectric photovoltaic effect; this was achieved by sandwiching lanthanum-modified lead zirconate titanate between two low work function metal electrodes. Using a similar concept, Zhu *et. al.* took advantage of a *piezo-phototronic* effect using a semiconducting piezoelectric (but non-ferroelectric) ZnO nanowire array on a silicon substrate to achieve enhanced efficiency[312]. Other examples include the fabrication of a multi-functional nano-generator using $PbZr_xTi_{1-x}O_3$ that was integrated with an air-driven nylon membrane and thermoelectric module[313], and the hybridization of electrical nano-generators and solar cells with supercapacitors for self-powered wearable electronic

textiles[314]. Park *et. al.* demonstrated a hybrid energy conversion system with integrated pyroelectric and thermoelectric modules to harvest solar energy across the full spectral range and demonstrated switching of electrochromic displays using the approach. In an analogous approach, Kim *et. al.* demonstrated enhanced energy collection by integrating a photothermal, pyroelectric and thermoelectric module with a solar cell.[315] A detailed state-of-the-art summary of nano-generator technologies based on mechanical (piezoelectric[316] and triboelectric[317]), thermal (pyroelectric[318] and thermoelectric[319]) and solar energy harvesting, their coupled mechanisms to harvest energy from multiple sources[320-324] and the possibilities of integrating energy harvesting devices with storage units[325, 326] can be found in the literature[309, 310]. However, these systems require distinct materials and, therefore, a more complex device structure is required, compared to a device operating on a single material, which is likely to increase losses. In contrast, a single material with an optimal combination of desired characteristics could enhance research effort in this direction.

To some extent most of the material property requirements for each application overlap with one another. Therefore, materials with overlapping desired properties for different applications could be used for a multiple energy conversion system. This will not only aid engineers and physicists in selecting an appropriate material from the existing pool of materials, but also provide insight for chemists and materials scientists for developing new materials. This could be achieved by employing appropriate materials selection techniques [327-333] or a detailed understanding of the individual material requirements, which are discussed in the following sub-sections. Similar approaches can be used to tune materials for a multiple energy conversion system.

8.1. Characteristics for hybrid perovskite solar cells

Initially, a suitable material for photovoltaic applications must have good light absorption, carrier generation, carrier lifetime and mobility [334-336]. The material should have a high

absorption coefficient, which governs the generation of free carriers or excitons subjected to the binding energy, temperature and carrier density[336]. A perovskite layer should have modest mobility[337] and a sufficiently high diffusion length which is a measurement of carrier transportation to the electrode before recombination[334]. In order to build efficient devices it is essential to optimize the film thickness and develop deposition and film treatment techniques for reliably producing good quality films[336]. It has been suggested that an appropriate selection of cations could facilitate spontaneous electrical polarization in these materials[100]. This will result in the creation of internal junctions at ferroelectric domains and help in the separation of photo-excited charge carriers. At the same time, the role of grain boundaries is also worth considering for enhanced ion transport.[338-344] Therefore, an improved knowledge of the fundamental ferroelectric nature of potential materials could significantly help in designing smart materials with better performance.[132] In addition, the presence of ferroelectric domains could aid in the reduction of segregation assisted recombination of charge carriers.[334] The transportation could be adversely affected by the presence of defects, which is often increased by doping since it enhances carrier scattering and thus influences conductivity, minority carrier lifetime and mobility. Doping not only affects the electrical transport, but also governs the operating mechanism of the device[336]. The attractive photovoltaic performance of hybrid halide perovskites is often attributed to a low density of trap defects [337, 345-347] or relatively shallow traps[348-350]. In addition, interface engineering that includes the development of alternate electron and hole transport materials or the use of doping can further improve the interface (morphologically and electrically) for charge transport[334]. Since the charge transport capability of a material also governs its suitability for supercapacitor and battery applications, any improvement to achieve better transport dynamics will also increase the suitability of these materials for supercapacitor and battery applications.

8.2. Characteristics for ferroelectric photovoltaics

As with the hybrid halide perovskites, the photovoltaic performance of ferroelectrics is also governed by light absorption, generation and separation of excitons, and the transportation dynamics of the charge carriers. Unlike the hybrid halide perovskites, ferroelectrics typically have a high band gap and low absorption coefficients. In this context, several attempts have been made to reduce their band gap and to enhance absorption using doping[351, 352], alloying[206] and oxygen vacancies[183, 353-355]. Though the presence of oxygen vacancies will enhance the conductivity of the ferroelectric and aid in charge transportation but a significant increase in conductivity will also lead to diminished ferroelectric polarization and enhanced leakage currents. Therefore, it is important to develop a trade-off between conductivity and polarization. In addition, the internal photoelectric effect can be used to enhance light absorption[180]. Although the absorption coefficient of ferroelectrics is typically low, their charge dissociation efficiency, due to a low binding energy, is high in contrast to hybrid halide perovskites. In general, ferroelectrics possess a high dielectric constant; which is inversely proportional to the binding energy of the excitons. However, the BPVE in ferroelectrics is governed by the non-centrosymmetric potential which is further dependent on the direction of polarization[356, 357]. The pre-decay shift in excited charge carriers is merely a few angstrom in the direction of polarization which results in small photocurrents.[43] Therefore, it becomes important to increase the non-centrosymmetry in ferroelectrics.[155, 215, 358, 359] The idea of enhancing the photocurrent by increasing the non-centrosymmetry is also supported by experiments.[360-362] For the final stage of charge collection, a reduction in the ferroelectric film thickness is beneficial, but the photovoltages are decreased.[151] Another method for increasing the collecting charge electric field is by forming an extended depletion layer using metal/intrinsic semiconductor/metal structures.[226] This could also be achieved by replacing the metal electrode with semiconductors which increases the depolarization field and charge collection efficiency by lowering the screening of spontaneous polarization.[145, 170]

The depolarization field is strongly dependent on the screening conditions at the interface and the film thickness.[95, 97, 98, 150] Therefore, interface engineering and film thickness optimization are essential for high photovoltaic responses of ferroelectrics.

8.3. Characteristics for thermo-electrical energy conversion and storage

The energy conversion using pyroelectric and thermoelectric effects could be termed as thermoelectrical energy conversion. For high pyroelectric energy conversion, the material should have a high pyroelectric coefficient to have a large change in polarization with respect to temperature fluctuation *(∂P/∂T)*. Consequently, dielectric anomalies, phase transitions or instantaneous switching, creation/destruction of crystal domains and the Curie temperature should lie within the operating temperature range. In addition, the materials should possess a high breakdown strength and high dielectric constant to achieve a large change in polarization with a variation in applied electric field. Importantly, it should exhibit low losses and leakage currents[15, 303, 363] [364]. Interestingly, the requirements for high pyroelectric energy conversion are similar to the requirements for high energy storage in ferroelectric capacitors[13]. As far as the requirements for thermoelectric energy conversions are concerned, ferroelectrics lie far behind the hybrid halide perovskites. However, to date no experimental study has confirmed the thermoelectric performance of the hybrid halide perovskites. Only theoretical calculations have been performed and suggestions have been made to tune the electrical conductivity. However, one report claims that using a $CaMnO_3$ ferroelectric buffer layer with a hybrid halide perovskite could help in increasing the open circuit voltage and provide a better thermoelectric output.[365] Similar attempts could help in creation of efficient energy conversion devices and makes it interesting to compile the materials requirements for possible multiple energy conversion devices.

8.4. Analogy in Material Requirements and Conclusions

There are theoretical reports where the pyroelectric effect is found to support the photovoltaic performance of the material.[366-368] Recently, the possibility of tuning piezoelectric[289], pyroelectric and dielectric properties by illumination has been demonstrated.[369, 370] Moreover, it is also possible to take advantage of piezoelectricity to enhance pyroelectric[16, 23], solar cell performance[16] and the performance of self-powered photodetectors. Interestingly, the ideal material requirements for photovoltaics are the same as for supercapacitor and battery applications. The same requirements of a tuned electrical conductivity also make a hybrid halide perovskite suitable for thermoelectric applications. In this context, the efforts of doping and creating an understanding of the effect of oxygen vacancies could be adopted from ferroelectrics. Importantly, the ideal properties for pyroelectric energy conversion and ferroelectric capacitors supplement photovoltaic effects in both ferroelectrics and perovskites. A stable hybrid organic-inorganic flexible ferroelectric material with a low band gap, high absorption coefficient and better charge transportation dynamics could become an excellent material for photovoltaic, supercapacitor and battery applications while a similar material with low thermal conductivity would be beneficial for thermoelectric effects. For pyroelectric energy conversion and ferroelectric capacitors, the leakage currents should be low and the existing properties with a high band gap, break-down strength and dielectric constant with low electrical conductivity in a hybrid organic-inorganic material could provide a better conversion efficiency and storage. Such perovskite materials with improved storage and conversion efficiencies could be integrated together for better utilization of available thermal and solar resource. Clearly, if multiple energy conversion mechanisms are anticipated there is a need to develop synergies in the multifunctional properties of these materials. In summary, the information compiled herewith is aimed at motivating researchers to realize the potential of existing perovskites and to develop novel hybrid halide ferroelectric perovskites for multiple energy conversion and storage systems.

Acknowledgements

RP acknowledge support from the Center of Excellence in Nanoelectronics (CEN), IIT Bombay, India. GV, JY, AHB and JS acknowledge support by the Australian Government via the Australian Research Council (ARC) through Discovery Grants and the Australian Renewable Energy Agency. CB acknowledges funding from the European Research Council under Grant Agreement no. 320963 on Novel Energy Materials, Engineering Science and Integrated Systems (NEMESIS).

Received: ((will be filled in by the editorial staff))
Revised: ((will be filled in by the editorial staff))
Published online: ((will be filled in by the editorial staff))

References

1. N.-G. Park, M. Grätzel, T. Miyasaka, K. Zhu, K. Emery, *Nature Energy* **2016**, *1*, 16152.
2. J. S. Manser, J. A. Christians, P. V. Kamat, *Chemical Reviews* **2016**, *116*, 12956-13008.
3. B. E. Hardin, H. J. Snaith, M. D. McGehee, *Nature Photonics* **2012**, *6*, 162-169.
4. H. J. Snaith, *The Journal of Physical Chemistry Letters* **2013**, *4*, 3623-3630.
5. M. A. Green, A. Ho-Baillie, H. J. Snaith, *Nature Photonics* **2014**, *8*, 506-514.
6. F. Giustino, H. J. Snaith, *ACS Energy Letters* **2016**.
7. N. A. Benedek, C. J. Fennie, *The Journal of Physical Chemistry C* **2013**, *117*, 13339-13349.
8. J. Young, P. Lalkiya, J. M. Rondinelli, *Journal of Materials Chemistry C* **2016**, *4*, 4016-4027.
9. W. Rehman, D. P. McMeekin, J. B. Patel, R. L. Milot, M. B. Johnston, H. J. Snaith, L. M. Herz, *Energy & Environmental Science* **2017**.
10. A. Chauhan, S. Patel, G. Vats, R. Vaish, *Energy Technology* **2014**, *2*, 205-209.
11. R. Sao, G. Vats, R. Vaish, *Ferroelectrics* **2015**, *474*, 1-7.
12. G. Vats, A. Chauhan, R. Vaish, *International Journal of Applied Ceramic Technology* **2015**, *12*, E49-E54.
13. G. Vats, H. S. Kushwaha, R. Vaish, *Materials Research Express* **2014**, *1*, 015503.
14. G. Vats, R. Vaish, C. R. Bowen, *Journal of Applied Physics* **2014**, *115*, 013505.
15. G. Vats, S. Patel, A. Chauhan, R. Vaish, *International Journal of Applied Ceramic Technology* **2015**, *12*, 765-770.
16. G. Vats, S. Patel, R. Vaish, *Integrated Ferroelectrics* **2016**, *168*, 69-84.
17. G. Vats, A. Kumar, N. Ortega, C. R. Bowen, R. S. Katiyar, *Energy & Environmental Science* **2016**, *9*, 1335-1345.

18. C. Bowen, H. Kim, P. Weaver, S. Dunn, *Energy & Environmental Science* **2014**, *7*, 25-44.
19. C. Bowen, J. Taylor, E. LeBoulbar, D. Zabek, A. Chauhan, R. Vaish, *Energy & Environmental Science* **2014**, *7*, 3836-3856
20. R. Kandilian, A. Navid, L. Pilon, *Smart Materials and Structures* **2011**, *20*, 055020.
21. F. Y. Lee, S. Goljahi, I. M. McKinley, C. S. Lynch, L. Pilon, *Smart Materials and Structures* **2012**, *21*, 025021.
22. F. Y. Lee, A. Navid, L. Pilon, *Applied Thermal Engineering* **2012**, *37*, 30-37.
23. I. M. McKinley, S. Goljahi, C. S. Lynch, L. Pilon, *Journal of Applied Physics* **2013**, *114*, 224111.
24. I. M. McKinley, R. Kandilian, L. Pilon, *Smart Materials and Structures* **2012**, *21*, 035015.
25. I. M. McKinley, F. Y. Lee, L. Pilon, *Applied energy* **2014**, *126*, 78-89.
26. A. Navid, L. Pilon, *Smart Materials and Structures* **2011**, *20*, 025012.
27. A. Navid, D. Vanderpool, A. Bah, L. Pilon, *International Journal of Heat And Mass Transfer* **2010**, *53*, 4060-4070.
28. D. Guyomar, S. Pruvost, G. Sebald, *Ultrasonics, Ferroelectrics and Frequency Control, IEEE Transactions on* **2008**, *55*, 279-285.
29. D. Guyomar, G. Sebald, E. Lefeuvre, A. Khodayari, *Journal of Intelligent Material Systems and Structures* **2009**, *20*, 265-271.
30. G. Sebald, D. Guyomar, A. Agbossou, *Smart Materials and Structures* **2009**, *18*, 125006.
31. G. Sebald, E. Lefeuvre, D. Guyomar, *Ultrasonics, Ferroelectrics and Frequency Control, IEEE Transactions on* **2008**, *55*, 538-551.
32. G. Sebald, S. Pruvost, D. Guyomar, *Smart Materials and Structures* **2008**, *17*, 015012.
33. G. Sebald, E. Lefeuvre, D. Guyomar, *IEEE Transactions on Ultrasonics, Ferroelectrics, and Frequency Control* **2008**, *55*.
34. A. Khodayari, S. Pruvost, G. Sebald, D. Guyomar, S. Mohammadi, *Ultrasonics, Ferroelectrics and Frequency Control, IEEE Transactions on* **2009**, *56*, 693-699.
35. H. Zhu, S. Pruvost, D. Guyomar, A. Khodayari, *Journal of Applied Physics* **2009**, *106*, 124102.
36. D. Guyomar, M. Lallart, presented at the Ultrasonics Symposium (IUS), 2009 IEEE International, 2009 (unpublished).
37. J. Seidel, D. Fu, S.-Y. Yang, E. Alarcón-Lladó, J. Wu, R. Ramesh, J. W. Ager III, *Physical Review Letters* **2011**, *107*, 126805.
38. S. Yang, J. Seidel, S. Byrnes, P. Shafer, C.-H. Yang, M. Rossell, P. Yu, Y.-H. Chu, J. Scott, J. Ager, *Nature Nanotechnology* **2010**, *5*, 143-147.
39. V. M. Fridkin, B. Popov, *Soviet Physics Uspekhi* **1978**, *21*, 981.
40. V. Fridkin, A. Grekov, P. Ionov, A. Rodin, E. Savchenko, K. Mikhailina, *Ferroelectrics* **1974**, *8*, 433-435.
41. V. Fridkin, *Applied Physics* **1977**, *13*, 357-359.
42. L. Belyaev, V. Fridkin, A. Grekov, N. Kosonogov, A. Rodin, *Le Journal de Physique Colloques* **1972**, *33*, C2-123-C122-125.
43. V. M. Fridkin, *Photoferroelectrics*. (Springer Science & Business Media, 1979).
44. J. E. Spanier, V. M. Fridkin, A. M. Rappe, A. R. Akbashev, A. Polemi, Y. Qi, Z. Gu, S. M. Young, C. J. Hawley, D. Imbrenda, *Nature Photonics* **2016**.
45. V. Fridkin, *Crystallography Reports* **2001**, *46*, 654-658.
46. B. I. Sturman, V. M. Fridkin, *Photovoltaic and photo-refractive effects in noncentrosymmetric materials*. (Gordon and Breach Publishers, 1992).
47. A. Zenkevich, Y. Matveyev, K. Maksimova, R. Gaynutdinov, A. Tolstikhina, V. Fridkin, *Physical Review B* **2014**, *90*, 161409.

48. A. Grekov, M. MA, V. Spitsyna, V. Fridkin, *Soviet physics crystallography, USSR* **1970**, *15*, 423-429.
49. Y. Bai, P. Tofel, J. Palosaari, H. Jantunen, J. Juuti, *Adv Mater* **2017**, *29*, 1700767.
50. I. Grinberg, D. V. West, M. Torres, G. Gou, D. M. Stein, L. Wu, G. Chen, E. M. Gallo, A. R. Akbashev, P. K. Davies, *Nature* **2013**, *503*, 509-512.
51. S. Lee, J. A. Bock, S. Trolier-McKinstry, C. A. Randall, *Journal of the European Ceramic Society* **2012**, *32*, 3971-3988.
52. Y. He, G. Galli, *Chemistry of Materials* **2014**, *26*, 5394-5400.
53. V. M. Goldschmidt, *Naturwissenschaften* **1926**, *14*, 477-485.
54. M. Johnsson, P. Lemmens, *Handbook of Magnetism and Advanced Magnetic Materials* **2007**.
55. P. Goudochnikov, A. J. Bell, *Journal of Physics: Condensed Matter* **2007**, *19*, 176201.
56. W. Li, Z. Wang, F. Deschler, S. Gao, R. H. Friend, A. K. Cheetham, *Nature Reviews Materials* **2017**, *2*, 16099.
57. G. Kieslich, S. Sun, A. K. Cheetham, *Chemical Science* **2014**, *5*, 4712-4715.
58. Z. Fan, K. Sun, J. Wang, *Journal of Materials Chemistry A* **2015**, *3*, 18809-18828.
59. Y. Yuan, Z. Xiao, B. Yang, J. Huang, *Journal of Materials chemistry A* **2014**, *2*, 6027-6041.
60. C. Paillard, X. Bai, I. C. Infante, M. Guennou, G. Geneste, M. Alexe, J. Kreisel, B. Dkhil, *Advanced Materials* **2016**, *28*, 5153-5168.
61. L. Pintilie, in *Ferroelectrics-Physical Effects* (InTech, 2011).
62. J. Seidel, L. W. Martin, Q. He, Q. Zhan, Y.-H. Chu, A. Rother, M. Hawkridge, P. Maksymovych, P. Yu, M. Gajek, *Nature materials* **2009**, *8*, 229.
63. J. Guyonnet, I. Gaponenko, S. Gariglio, P. Paruch, *Advanced Materials* **2011**, *23*, 5377-5382.
64. T. Sluka, A. K. Tagantsev, P. Bednyakov, N. Setter, *Nature communications* **2013**, *4*, 1808.
65. X. Qi, J. Dho, R. Tomov, M. G. Blamire, J. L. MacManus-Driscoll, *Applied Physics Letters* **2005**, *86*, 062903.
66. G. W. Pabst, L. W. Martin, Y.-H. Chu, R. Ramesh, *Applied Physics Letters* **2007**, *90*, 072902.
67. M. Raymond, D. Smyth, *Journal of Physics and Chemistry of Solids* **1996**, *57*, 1507-1511.
68. T. M. Brenner, D. A. Egger, L. Kronik, G. Hodes, D. Cahen, *Nature Reviews Materials* **2016**, *1*, 15007.
69. A. Zakutayev, C. M. Caskey, A. N. Fioretti, D. S. Ginley, J. Vidal, V. Stevanovic, E. Tea, S. Lany, *The journal of physical chemistry letters* **2014**, *5*, 1117-1125.
70. A. Walsh, A. Zunger, *Nature materials* **2017**, *16*, 964.
71. Y. Liu, L. Collins, R. Proksch, S. Kim, B. R. Watson, B. Doughty, T. R. Calhoun, M. Ahmadi, A. V. Ievlev, S. Jesse, *Nature materials* **2018**, 1.
72. A. Stroppa, D. Di Sante, P. Barone, M. Bokdam, G. Kresse, C. Franchini, M.-H. Whangbo, S. Picozzi, *Nature Communications* **2014**, *5*, 5900.
73. J. Even, L. Pedesseau, J.-M. Jancu, C. Katan, *The Journal of Physical Chemistry Letters* **2013**, *4*, 2999-3005.
74. E. Mosconi, P. Umari, F. De Angelis, *Physical Chemistry Chemical Physics* **2016**, *18*, 27158-27164.
75. F. Brivio, K. T. Butler, A. Walsh, M. Van Schilfgaarde, *Physical Review B* **2014**, *89*, 155204.
76. T. Wang, B. Daiber, J. M. Frost, S. A. Mann, E. C. Garnett, A. Walsh, B. Ehrler, *Energy & Environmental Science* **2017**, *10*, 509-515.

77. T. Etienne, E. Mosconi, F. De Angelis, *The Journal of Physical Chemistry Letters* **2016**, *7*, 1638-1645.
78. E. J. Juarez-Perez, R. S. Sanchez, L. Badia, G. Garcia-Belmonte, Y. S. Kang, I. Mora-Sero, J. Bisquert, *The journal of physical chemistry letters* **2014**, *5*, 2390-2394.
79. N. A. Hill, (ACS Publications, 2000).
80. N. A. Benedek, C. J. Fennie, *Physical review letters* **2011**, *106*, 107204.
81. M. Senn, D. Keen, T. Lucas, J. Hriljac, A. Goodwin, *Physical Review Letters* **2016**, *116*, 207602.
82. R. E. Cohen, *Nature* **1992**, *358*, 136-138.
83. J. Neaton, C. Ederer, U. Waghmare, N. Spaldin, K. Rabe, *Physical Review B* **2005**, *71*, 014113.
84. E. H. Smith, N. A. Benedek, C. J. Fennie, *Inorganic Chemistry* **2015**, *54*, 8536-8543.
85. H. J. Zhao, J. Íñiguez, W. Ren, X. M. Chen, L. Bellaiche, *Physical Review B* **2014**, *89*, 174101.
86. J. M. Frost, K. T. Butler, A. Walsh, *APL Materials* **2014**, *2*, 081506.
87. M. T. Weller, O. J. Weber, P. F. Henry, A. M. Di Pumpo, T. C. Hansen, *Chemical Communications* **2015**, *51*, 4180-4183.
88. Y. Rakita, E. Meirzadeh, T. Bendikov, V. Kalchenko, I. Lubomirsky, G. Hodes, D. Ehre, D. Cahen, *APL Materials* **2016**, *4*, 051101.
89. Y. Rakita, O. Bar-Elli, E. Meirzadeh, H. Kaslasi, Y. Peleg, G. Hodes, I. Lubomirsky, D. Oron, D. Ehre, D. Cahen, *Proceedings of the National Academy of Sciences* **2017**, 201702429.
90. M. Ikura, *Ferroelectrics* **2002**, *267*, 403-408.
91. L. Kouchachvili, M. Ikura, *International Journal of Energy Research* **2008**, *32*, 328-335.
92. R. Whatmore, *Ferroelectrics* **1991**, *118*, 241-259.
93. R. Whatmore, *Reports on progress in physics* **1986**, *49*, 1335.
94. M. Xie, Y. Zhang, M. J. Kraśny, C. Bowen, H. Khanbareh, N. Gathercole, *Energy & Environmental Science* **2018**.
95. R. Mehta, B. Silverman, J. Jacobs, *Journal of Applied Physics* **1973**, *44*, 3379-3385.
96. P. Lopez-Varo, L. Bertoluzzi, J. Bisquert, M. Alexe, M. Coll, J. Huang, J. A. Jimenez-Tejada, T. Kirchartz, R. Nechache, F. Rosei, *Physics Reports* **2016**, *653*, 1-40.
97. I. Batra, P. Wurfel, B. Silverman, *Physical Review B* **1973**, *8*, 3257.
98. P. Wurfel, I. Batra, *Physical Review B* **1973**, *8*, 5126.
99. D. Lee, S. Baek, T. Kim, J.-G. Yoon, C. Folkman, C. Eom, T. Noh, *Physical Review B* **2011**, *84*, 125305.
100. J. M. Frost, K. T. Butler, F. Brivio, C. H. Hendon, M. Van Schilfgaarde, A. Walsh, *Nano Letters* **2014**, *14*, 2584-2590.
101. Y. Kutes, L. Ye, Y. Zhou, S. Pang, B. D. Huey, N. P. Padture, *The Journal of Physical Chemistry Letters* **2014**, *5*, 3335-3339.
102. , 2015.
103. M. A. Green, *Solar cells: operating principles, technology, and system applications*. (Englewood Cliffs, NJ, Prentice-Hall, Inc., 1982. 288 p., 1982).
104. A. Fahrenbruch, R. Bube, *Fundamentals of solar cells: photovoltaic solar energy conversion*. (Elsevier, 2012).
105. B. A. Gregg, *The Journal of Physical Chemistry B* **2003**, *107*, 4688-4698.
106. B. O'regan, M. Grätzel, *Nature* **1991**, *353*, 737-740.
107. S. Ardo, G. J. Meyer, *Chemical Society Reviews* **2009**, *38*, 115-164.
108. E. Edri, S. Kirmayer, A. Henning, S. Mukhopadhyay, K. Gartsman, Y. Rosenwaks, G. Hodes, D. Cahen, *Nano letters* **2014**, *14*, 1000-1004.

109. V. D'Innocenzo, G. Grancini, M. J. Alcocer, A. R. S. Kandada, S. D. Stranks, M. M. Lee, G. Lanzani, H. J. Snaith, A. Petrozza, *Nature communications* **2014**, *5*, 3586.
110. M. Hirasawa, T. Ishihara, T. Goto, K. Uchida, N. Miura, *Physica B: Condensed Matter* **1994**, *201*, 427-430.
111. K. Tanaka, T. Takahashi, T. Ban, T. Kondo, K. Uchida, N. Miura, *Solid state communications* **2003**, *127*, 619-623.
112. W. S. Yang, B.-W. Park, E. H. Jung, N. J. Jeon, Y. C. Kim, D. U. Lee, S. S. Shin, J. Seo, E. K. Kim, J. H. Noh, *Science* **2017**, *356*, 1376-1379.
113. J. Burschka, N. Pellet, S.-J. Moon, R. Humphry-Baker, P. Gao, M. K. Nazeeruddin, M. Grätzel, *Nature* **2013**, *499*, 316.
114. N. J. Jeon, J. H. Noh, W. S. Yang, Y. C. Kim, S. Ryu, J. Seo, S. I. Seok, *Nature* **2015**, *517*, 476.
115. C.-S. Jiang, M. Yang, Y. Zhou, B. To, S. U. Nanayakkara, J. M. Luther, W. Zhou, J. J. Berry, J. Van De Lagemaat, N. P. Padture, *Nature communications* **2015**, *6*, 8397.
116. V. W. Bergmann, S. A. Weber, F. J. Ramos, M. K. Nazeeruddin, M. Grätzel, D. Li, A. L. Domanski, I. Lieberwirth, S. Ahmad, R. Berger, *Nature communications* **2014**, *5*, 5001.
117. M. A. Green, S. P. Bremner, *Nature Materials* **2017**, *16*, 23-34.
118. F. Hao, C. C. Stoumpos, D. H. Cao, R. P. Chang, M. G. Kanatzidis, *Nature Photonics* **2014**, *8*, 489-494.
119. S. Wang, Y. Jiang, E. J. Juarez-Perez, L. K. Ono, Y. Qi, *Nature Energy* **2016**, *2*, 16195.
120. S. S. Shin, E. J. Yeom, W. S. Yang, S. Hur, M. G. Kim, J. Im, J. Seo, J. H. Noh, S. I. Seok, *Science* **2017**, *356*, 167-171.
121. B. Chen, J. Shi, X. Zheng, Y. Zhou, K. Zhu, S. Priya, *Journal of Materials Chemistry A* **2015**, *3*, 7699-7705.
122. Z. Sun, X. Liu, T. Khan, C. Ji, M. A. Asghar, S. Zhao, L. Li, M. Hong, J. Luo, *Angewandte Chemie* **2016**, *128*, 6655-6660.
123. P.-F. Li, Y.-Y. Tang, Z.-X. Wang, H.-Y. Ye, Y.-M. You, R.-G. Xiong, *Nature Communications* **2016**, *7*, 13635.
124. H.-W. Chen, N. Sakai, M. Ikegami, T. Miyasaka, *The Journal of Physical Chemistry Letters* **2014**, *6*, 164-169.
125. Z. Fan, J. Xiao, K. Sun, L. Chen, Y. Hu, J. Ouyang, K. P. Ong, K. Zeng, J. Wang, *The Journal of Physical Chemistry Letters* **2015**, *6*, 1155-1161.
126. G. A. Sewvandi, K. Kodera, H. Ma, S. Nakanishi, Q. Feng, *Scientific Reports* **2016**, *6*.
127. S. N. Rashkeev, F. El-Mellouhi, S. Kais, F. H. Alharbi, *Scientific Reports* **2015**, *5*.
128. D.-F. Pan, G.-F. Bi, G.-Y. Chen, H. Zhang, J.-M. Liu, G.-H. Wang, J.-G. Wan, *Scientific Reports* **2016**, *6*.
129. E. Strelcov, Q. Dong, T. Li, J. Chae, Y. Shao, Y. Deng, A. Gruverman, J. Huang, A. Centrone, *Science Advances* **2017**, *3*, e1602165.
130. M. N. F. Hoque, M. Yang, Z. Li, N. Islam, X. Pan, K. Zhu, Z. Fan, *ACS Energy Letters* **2016**, *1*, 142-149.
131. P. Wang, J. Zhao, L. Wei, Q. Zhu, S. Xie, J. Liu, X. Meng, J. Li, *Nanoscale* **2017**, *9*, 3806-3817.
132. H. Röhm, T. Leonhard, M. J. Hoffmann, A. Colsmann, *Energy & Environmental Science* **2017**, *10*, 950-955
133. A. Alsubaie, P. Sharma, J. H. Lee, J. Y. Kim, C.-H. Yang, J. Seidel, *ACS applied materials & interfaces* **2018**, *10*, 11768-11775.
134. A. Alsubaie, P. Sharma, G. Liu, V. Nagarajan, J. Seidel, *Nanotechnology* **2017**, *28*, 075709.

135. S. Hu, A. Alsubaie, Y. Wang, J. H. Lee, K. R. Kang, C. H. Yang, J. Seidel, *physica status solidi (a)* **2017**, *214*, 1600356.
136. P. S. Brody, F. Crowne, *Journal of Electronic Materials* **1975**, *4*, 955-971.
137. E. Krätzig, H. Kurz, *Ferroelectrics* **1976**, *13*, 295-296.
138. K. T. Butler, J. M. Frost, A. Walsh, *Energy & Environmental Science* **2015**, *8*, 838-848.
139. Y. Jiang, X. Wen, A. Benda, R. Sheng, A. W. Ho-Baillie, S. Huang, F. Huang, Y.-B. Cheng, M. A. Green, *Solar Energy Materials and Solar Cells* **2016**, *151*, 102-112.
140. W. Ji, K. Yao, Y. C. Liang, *Advanced Materials* **2010**, *22*, 1763-1766.
141. M. Alexe, D. Hesse, *Nature Communications* **2011**, *2*, 256.
142. A. Bhatnagar, A. R. Chaudhuri, Y. H. Kim, D. Hesse, M. Alexe, *Nature Communications* **2013**, *4*.
143. J. Kreisel, M. Alexe, P. A. Thomas, *Nature Materials* **2012**, *11*, 260-260.
144. D. Daranciang, M. J. Highland, H. Wen, S. M. Young, N. C. Brandt, H. Y. Hwang, M. Vattilana, M. Nicoul, F. Quirin, J. Goodfellow, *Physical Review Letters* **2012**, *108*, 087601.
145. M. Qin, K. Yao, Y. C. Liang, *Applied Physics Letters* **2008**, *93*, 122904.
146. A. M. Prokhorov, *Ferroelectric crystals for laser radiation control*. (Taylor & Francis, 1990).
147. P. S. Brody, *Applied Physics Letters* **1981**, *38*, 153-155.
148. L. Pintilie, I. Vrejoiu, G. Le Rhun, M. Alexe, *Journal of Applied Physics* **2007**, *101*, 064109.
149. P. Brody, *Solid State Communications* **1973**, *12*, 673-676.
150. M. Qin, K. Yao, Y. C. Liang, S. Shannigrahi, *Journal of Applied Physics* **2007**, *101*, 014104.
151. M. Ichiki, R. Maeda, Y. Morikawa, Y. Mabune, T. Nakada, K. Nonaka, *Applied Physics Letters* **2004**, *84*, 395-397.
152. M. Ichiki, H. Furue, T. Kobayashi, R. Maeda, Y. Morikawa, T. Nakada, K. Nonaka, *Applied Physics Letters* **2005**, *87*, 222903.
153. M. Ichiki, Y. Morikawa, Y. Mabune, T. Nakada, *Journal of the European Ceramic Society* **2004**, *24*, 1709-1714.
154. A. Glass, D. Von der Linde, T. Negran, *Applied Physics Letters* **1974**, *25*, 233-235.
155. S. M. Young, A. M. Rappe, *Physical Review Letters* **2012**, *109*, 116601.
156. S. M. Young, F. Zheng, A. M. Rappe, *Physical Review Letters* **2012**, *109*, 236601.
157. F. Zheng, H. Takenaka, F. Wang, N. Z. Koocher, A. M. Rappe, *The Journal of Physical Chemistry Letters* **2014**, *6*, 31-37.
158. S. M. Young, F. Zheng, A. M. Rappe, *Physical Review Letters* **2013**, *110*, 057201.
159. L. Z. Tan, F. Zheng, S. M. Young, F. Wang, S. Liu, A. M. Rappe, *NPJ Computational Materials* **2016**, *2*, 16026.
160. R. von Baltz, W. Kraut, *Physical Review B* **1981**, *23*, 5590.
161. R. Guo, L. You, Y. Zhou, Z. S. Lim, X. Zou, L. Chen, R. Ramesh, J. Wang, *Nature Communications* **2013**, *4*.
162. P. Gunter, *Ferroelectrics* **1978**, *22*, 671-674.
163. Z. Wu, Y. Zhang, K. Ma, Y. Cao, H. Lin, Y. Jia, J. Chen, H. Li, *Physica Status Solidi (RRL)-Rapid Research Letters* **2014**, *8*, 36-39.
164. B. Fregoso, T. Morimoto, J. E Moore, *Bulletin of the American Physical Society* **2017**, *62*.
165. A. Chynoweth, *Physical Review* **1956**, *102*, 705.
166. L. Pensak, *Physical Review* **1958**, *109*, 601.
167. B. Goldstein, L. Pensak, *Journal of Applied Physics* **1959**, *30*, 155-161.
168. B. Goldstein, *Physical Review* **1958**, *109*, 601.

169. S. Ellis, F. Herman, E. Loebner, W. Merz, C. Struck, J. White, *Physical Review* **1958**, *109*, 1860.
170. B. Chen, M. Li, Y. Liu, Z. Zuo, F. Zhuge, Q.-F. Zhan, R.-W. Li, *Nanotechnology* **2011**, *22*, 195201.
171. B. Chen, Z. Zuo, Y. Liu, Q.-F. Zhan, Y. Xie, H. Yang, G. Dai, Z. Li, G. Xu, R.-W. Li, *Applied Physics Letters* **2012**, *100*, 173903.
172. W. Dong, Y. Guo, B. Guo, H. Liu, H. Li, H. Liu, *Materials Letters* **2013**, *91*, 359-361.
173. L. Pintilie, M. Alexe, *Journal of Applied Physics* **2005**, *98*, 124103.
174. M. Y. Zhuravlev, R. F. Sabirianov, S. Jaswal, E. Y. Tsymbal, *Physical Review Letters* **2005**, *94*, 246802.
175. D. Pantel, M. Alexe, *Physical Review B* **2010**, *82*, 134105.
176. C. Ahn, K. Rabe, J.-M. Triscone, *Science* **2004**, *303*, 488-491.
177. M. Qin, K. Yao, Y. C. Liang, *Applied Physics Letters* **2009**, *95*, 022912.
178. M. Ichiki, Y. Morikawa, T. Nakada, *Japanese Journal of Applied Physics* **2002**, *41*, 6993.
179. P. Brody, *Solid State Communications* **1973**, *12*, 673-676.
180. J. Zhang, X. Su, M. Shen, Z. Dai, L. Zhang, X. He, W. Cheng, M. Cao, G. Zou, *Scientific Reports* **2013**, *3*.
181. M. Qin, K. Yao, Y. C. Liang, *Journal of Applied Physics* **2009**, *105*, 061624.
182. M. Qin, K. Yao, Y. C. Liang, B. K. Gan, *Applied Physics Letters* **2007**, *91*, 092904.
183. H. Yi, T. Choi, S. Choi, Y. S. Oh, S. W. Cheong, *Advanced Materials* **2011**, *23*, 3403-3407.
184. P. Zhang, D. Cao, C. Wang, M. Shen, X. Su, L. Fang, W. Dong, F. Zheng, *Materials Chemistry and Physics* **2012**, *135*, 304-308.
185. K. Yao, B. K. Gan, M. Chen, S. Shannigrahi, *Applied Physics Letters* **2005**, *87*, 212906.
186. Z. Fan, W. Ji, T. Li, J. Xiao, P. Yang, K. P. Ong, K. Zeng, K. Yao, J. Wang, *Acta Materialia* **2015**, *88*, 83-90.
187. L. Fang, L. You, Y. Zhou, P. Ren, Z. Shiuh Lim, J. Wang, *Applied Physics Letters* **2014**, *104*, 142903.
188. P. Blom, R. Wolf, J. Cillessen, M. Krijn, *Physical Review Letters* **1994**, *73*, 2107.
189. Y. Guo, B. Guo, W. Dong, H. Li, H. Liu, *Nanotechnology* **2013**, *24*, 275201.
190. Z. Xiao, Y. Yuan, Y. Shao, Q. Wang, Q. Dong, C. Bi, P. Sharma, A. Gruverman, J. Huang, *Nature Materials* **2015**, *14*, 193-198.
191. Y. Zhao, C. Liang, H. Zhang, D. Li, D. Tian, G. Li, X. Jing, W. Zhang, W. Xiao, Q. Liu, *Energy & Environmental Science* **2015**, *8*, 1256-1260.
192. F. Zheng, J. Xu, L. Fang, M. Shen, X. Wu, *Applied Physics Letters* **2008**, *93*, 172101.
193. J. Seidel, *The Journal of Physical Chemistry Letters* **2012**, *3*, 2905-2909.
194. H. Huang, *Nature Photonics* **2010**, *4*, 134-135.
195. J. Seidel, G. Singh-Bhalla, Q. He, S.-Y. Yang, Y.-H. Chu, R. Ramesh, *Phase Transitions* **2013**, *86*, 53-66.
196. Y. P. Chiu, Y. T. Chen, B. C. Huang, M. C. Shih, J. C. Yang, Q. He, C. W. Liang, J. Seidel, Y. C. Chen, R. Ramesh, *Advanced Materials* **2011**, *23*, 1530-1534.
197. J. Seidel, P. Maksymovych, Y. Batra, A. Katan, S.-Y. Yang, Q. He, A. P. Baddorf, S. V. Kalinin, C.-H. Yang, J.-C. Yang, *Physical Review Letters* **2010**, *105*, 197603.
198. J. Seidel, S.-Y. Yang, E. Alarcòn-Lladò, J. Ager III, R. Ramesh, *Ferroelectrics* **2012**, *433*, 123-126.
199. H. Matsuo, Y. Kitanaka, R. Inoue, Y. Noguchi, M. Miyayama, T. Kiguchi, T. J. Konno, *Physical Review B* **2016**, *94*, 214111.
200. C. Blouzon, J. Chauleau, A. Mougin, S. Fusil, M. Viret, *Physical Review B* **2016**, *94*, 094107.

201. R. Inoue, S. Ishikawa, R. Imura, Y. Kitanaka, T. Oguchi, Y. Noguchi, M. Miyayama, *Scientific Reports* **2015**, *5*.
202. H.-J. Feng, M. Wang, F. Liu, B. Duan, J. Tian, X. Guo, *Journal of Alloys and Compounds* **2015**, *628*, 311-316.
203. S. Liu, F. Zheng, N. Z. Koocher, H. Takenaka, F. Wang, A. M. Rappe, *The Journal of Physical Chemistry Letters* **2015**, *6*, 693-699.
204. A. Lubk, S. Gemming, N. Spaldin, *Physical Review B* **2009**, *80*, 104110.
205. O. Diéguez, P. Aguado-Puente, J. Junquera, J. Íñiguez, *Physical Review B* **2013**, *87*, 024102.
206. W. S. Choi, M. F. Chisholm, D. J. Singh, T. Choi, G. E. Jellison Jr, H. N. Lee, *Nature Communications* **2012**, *3*, 689.
207. J. C. Wojdeł, J. Iniguez, *Physical Review Letters* **2014**, *112*, 247603.
208. A. Kudo, Y. Miseki, *Chemical Society Reviews* **2009**, *38*, 253-278.
209. A. Haussmann, P. Milde, C. Erler, L. M. Eng, *Nano Letters* **2009**, *9*, 763-768.
210. F. Yan, G. Chen, L. Lu, J. E. Spanier, *ACS Nano* **2012**, *6*, 2353-2360.
211. T. Choi, L. Jiang, S. Lee, T. Egami, H. N. Lee, *New Journal of Physics* **2012**, *14*, 093056.
212. L. Pintilie, C. Dragoi, I. Pintilie, *Journal of Applied Physics* **2011**, *110*, 044105.
213. T. Qu, Y. Zhao, D. Xie, J. Shi, Q. Chen, T. Ren, *Applied Physics Letters* **2011**, *98*, 173507.
214. C. Tu, C. Hung, V. Schmidt, R. Chien, M. Jiang, J. Anthoninappen, *Journal of Physics: Condensed Matter* **2012**, *24*, 495902.
215. G. Gopal Khan, R. Das, N. Mukherjee, K. Mandal, *physica status solidi (RRL)-Rapid Research Letters* **2012**, *6*, 312-314.
216. X. Zhang, H. Liu, B. Zheng, Y. Lin, D. Liu, C.-W. Nan, *Journal of Nanomaterials* **2013**, *2013*, 3.
217. L. Wang, K. Wang, B. Zou, *The Journal of Physical Chemistry Letters* **2016**, *7*, 2556-2562.
218. R. Nechache, C. Harnagea, S. Li, L. Cardenas, W. Huang, J. Chakrabartty, F. Rosei, *Nature Photonics* **2015**, *9*, 61.
219. J. Chakrabartty, C. Harnagea, M. Celikin, F. Rosei, R. Nechache, *Nature Photonics* **2018**, *12*, 271.
220. R. Nechache, C. Harnagea, S. Licoccia, E. Traversa, A. Ruediger, A. Pignolet, F. Rosei, *Applied Physics Letters* **2011**, *98*, 202902.
221. V. Yarmarkin, B. Gol'tsman, M. Kazanin, V. Lemanov, *Physics of the Solid State* **2000**, *42*, 522-527.
222. T. Choi, S. Lee, Y. Choi, V. Kiryukhin, S.-W. Cheong, *Science* **2009**, *324*, 63-66.
223. S. Yang, L. Martin, S. Byrnes, T. Conry, S. Basu, D. Paran, L. Reichertz, J. Ihlefeld, C. Adamo, A. Melville, *Applied Physics Letters* **2009**, *95*, 062909.
224. T. Qu, Y. Zhao, D. Xie, J. Shi, Q. Chen, T. Ren, *Applied Physics Letters* **2011**, *98*, 173507.
225. D. Cao, C. Wang, F. Zheng, W. Dong, L. Fang, M. Shen, *Nano Letters* **2012**, *12*, 2803-2809.
226. Y. Zang, D. Xie, X. Wu, Y. Chen, Y. Lin, M. Li, H. Tian, X. Li, Z. Li, H. Zhu, *Applied Physics Letters* **2011**, *99*, 132904.
227. R. Katiyar, A. Kumar, G. Morell, J. Scott, R. Katiyar, *Applied Physics Letters* **2011**, *99*, 092906.
228. H. Goldsmid, *Thermoelectric refrigeration*. (Springer, 2013).
229. H. J. Goldsmid, **1960**.
230. T. Tritt, *Recent Trends in Thermoelectric Materials Research, Part Two*. (Academic Press, 2000).

231. S. Lee, R. H. Wilke, S. Trolier-McKinstry, S. Zhang, C. A. Randall, *Applied Physics Letters* **2010**, *96*, 031910.
232. S. Lee, S. Dursun, C. Duran, C. A. Randall, *Journal of Materials Research* **2011**, *26*, 26-30.
233. T. Okuda, K. Nakanishi, S. Miyasaka, Y. Tokura, *Physical Review B* **2001**, *63*, 113104.
234. H. Frederikse, W. Thurber, W. Hosler, *Physical Review* **1964**, *134*, A442.
235. H. Ohta, *Materials Today* **2007**, *10*, 44-49.
236. B. Jalan, S. Stemmer, *Applied Physics Letters* **2010**, *97*, 042106.
237. C. Yu, M. L. Scullin, M. Huijben, R. Ramesh, A. Majumdar, *Applied Physics Letters* **2008**, *92*, 092118.
238. H. Muta, K. Kurosaki, S. Yamanaka, *Journal of Alloys and Compounds* **2003**, *350*, 292-295.
239. M. L. Scullin, J. Ravichandran, C. Yu, M. Huijben, J. Seidel, A. Majumdar, R. Ramesh, *Acta Materialia* **2010**, *58*, 457-463.
240. M. L. Scullin, C. Yu, M. Huijben, S. Mukerjee, J. Seidel, Q. Zhan, J. Moore, A. Majumdar, R. Ramesh, *Applied Physics Letters* **2008**, *92*, 202113.
241. M. Ohtaki, H. Koga, T. Tokunaga, K. Eguchi, H. Arai, *Journal of Solid State Chemistry* **1995**, *120*, 105-111.
242. R. Kabir, T. Zhang, D. Wang, R. Donelson, R. Tian, T. T. Tan, S. Li, *Journal of Materials Science* **2014**, *49*, 7522-7528.
243. F. Zhang, Q. Lu, X. Zhang, J. Zhang, *Journal of Physics and Chemistry of Solids* **2013**, *74*, 1859-1864.
244. Y. Chen, Y. Zhao, Z. Liang, *Energy & Environmental Science* **2015**, *8*, 401-422.
245. B. Russ, A. Glaudell, J. J. Urban, M. L. Chabinyc, R. A. Segalman, *Nature Reviews Materials* **2016**, *1*, 16050.
246. X. Mettan, R. Pisoni, P. Matus, A. Pisoni, J. i. Jaćimović, B. Náfrádi, M. Spina, D. Pavuna, L. Forró, E. Horváth, *The Journal of Physical Chemistry C* **2015**, *119*, 11506-11510.
247. C. Lee, J. Hong, A. Stroppa, M.-H. Whangbo, J. H. Shim, *RSC Advances* **2015**, *5*, 78701-78707.
248. A. Filippetti, C. Caddeo, P. D. Delugas, A. Mattoni, *The Journal of Physical Chemistry C* **2016**.
249. M. Wang, S. Lin, *Advanced Functional Materials* **2016**, *26*, 5297-5306.
250. T. Zhao, D. Wang, Z. Shuai, *Synthetic Metals* **2017**, *225*, 108-114.
251. Z. Yao, Z. Song, H. Hao, Z. Yu, M. Cao, S. Zhang, M. T. Lanagan, H. Liu, *Advanced Materials* **2017**.
252. J. Scott, *Science* **2007**, *315*, 954-959.
253. P. Kim, N. M. Doss, J. P. Tillotson, P. J. Hotchkiss, M.-J. Pan, S. R. Marder, J. Li, J. P. Calame, J. W. Perry, *ACS Nano* **2009**, *3*, 2581-2592.
254. V. Tomer, G. Polizos, E. Manias, C. Randall, *Journal of Applied Physics* **2010**, *108*, 074116.
255. V. Tomer, E. Manias, C. Randall, *Journal of Applied Physics* **2011**, *110*, 044107.
256. I. Burn, D. Smyth, *Journal of Materials Science* **1972**, *7*, 339-343.
257. G. R. Love, *Journal of the American Ceramic Society* **1990**, *73*, 323-328.
258. H. Huang, J. F. Scott, *Ferroelectric Materials for Energy Applications*. (John Wiley & Sons, 2018).
259. Q. Li, F.-Z. Yao, Y. Liu, G. Zhang, H. Wang, Q. Wang, *Annual Review of Materials Research* **2018**.
260. L. Yang, X. Kong, F. Li, H. Hao, Z. Cheng, H. Liu, J.-F. Li, S. Zhang, *Progress in Materials Science* **2018**.

261. H. Palneedi, M. Peddigari, G. T. Hwang, D. Y. Jeong, J. Ryu, *Advanced Functional Materials* **2018**, *28*, 1803665.
262. Z. Liu, T. Lu, J. Ye, G. Wang, X. Dong, R. Withers, Y. Liu, *Advanced Materials Technologies* **2018**, *3*, 1800111.
263. Q. Chen, Y. Shen, S. Zhang, Q. Zhang, *Annual review of materials research* **2015**, *45*, 433-458.
264. X. Hao, *Journal of Advanced Dielectrics* **2013**, *3*, 1330001.
265. N. Ortega, A. Kumar, J. Scott, D. B. Chrisey, M. Tomazawa, S. Kumari, D. Diestra, R. Katiyar, *Journal of Physics: Condensed Matter* **2012**, *24*, 445901.
266. W. Zhang, G. E. Eperon, H. J. Snaith, *Nature Energy* **2016**, *1*, 16048.
267. J. Beilsten-Edmands, G. Eperon, R. Johnson, H. Snaith, P. Radaelli, *Applied Physics Letters* **2015**, *106*, 173502.
268. S. Zhou, L. Li, H. Yu, J. Chen, C. P. Wong, N. Zhao, *Advanced Electronic Materials* **2016**, *2*, 1600114 (1600111-1600118).
269. J. K. Pious, M. Lekshmi, C. Muthu, R. Rakhi, V. C. Nair, *ACS Omega* **2017**, *2*, 5798-5802.
270. D. Kim, J. S. Yun, P. Sharma, D. S. Lee, J. Kim, A. M. Soufiani, S. Huang, M. A. Green, A. W. Y. Ho-Baillie, J. Seidel, *Nature Communications* **2019**, *10*, 444.
271. M. Winter, R. J. Brodd, (ACS Publications, 2004).
272. H. Kim, J. S. Han, J. Choi, S. Y. Kim, H. W. Jang, *Small Methods* **2018**, *2*, 1700310.
273. H.-R. Xia, W.-T. Sun, L.-M. Peng, *Chemical Communications* **2015**, *51*, 13787-13790.
274. N. Vicente, G. Garcia-Belmonte, *Advanced Energy Materials* **2017**, *7*, 1700710.
275. M. Tathavadekar, S. Krishnamurthy, A. Banerjee, S. Nagane, Y. Gawli, A. Suryawanshi, S. Bhat, D. Puthusseri, A. D. Mohite, S. Ogale, *Journal of Materials Chemistry A* **2017**, *5*, 18634-18642.
276. S. Ahmad, C. George, D. J. Beesley, J. J. Baumberg, M. De Volder, *Nano letters* **2018**, *18*, 1856-1862.
277. D. Ramirez, Y. Suto, N. C. Rosero-Navarro, A. Miura, K. Tadanaga, F. Jaramillo, *Inorganic chemistry* **2018**, *57*, 4181-4188.
278. Q. Wang, T. Yang, H. Wang, J. Zhang, X. Guo, Z. Yang, S. Lu, W. Qin, *CrystEngComm* **2019**.
279. Y. Shao, Y. Fang, T. Li, Q. Wang, Q. Dong, Y. Deng, Y. Yuan, H. Wei, M. Wang, A. Gruverman, *Energy & Environmental Science* **2016**, *9*, 1752-1759.
280. T. Miyasaka, T. N. Murakami, *Applied Physics Letters* **2004**, *85*, 3932-3934.
281. R. Liu, C. Liu, S. Fan, *Journal of Materials Chemistry A* **2017**, *5*, 23078-23084.
282. C. H. Ng, H. N. Lim, S. Hayase, Z. Zainal, S. Shafie, H. W. Lee, N. M. Huang, *ACS Applied Energy Materials* **2018**, *1*, 692-699.
283. G.-L. Liou, C.-H. Cheng, Y.-C. Chiu, presented at the Electron Devices and Solid-State Circuits (EDSSC), 2017 International Conference on, 2017 (unpublished).
284. A. Bogusz, O. Choudhary, I. Skorupa, D. Bürger, A. Lawerenz, Y. Lei, H. Zeng, B. Abendroth, H. Stöcker, O. Schmidt, *Applied Physics Letters* **2016**, *108*, 052103.
285. C.-W. Lo, C. Li, H. Jiang, *Aip Advances* **2011**, *1*, 042104.
286. F. Rubio-Marcos, D. A. Ochoa, A. Del Campo, M. A. García, G. R. Castro, J. F. Fernández, J. E. García, *Nature Photonics* **2018**, *12*, 29.
287. Y. Bai, G. Vats, J. Seidel, H. Jantunen, J. Juuti, *Advanced Materials* **2018**.
288. Y.-J. Kim, T.-V. Dang, H.-J. Choi, B.-J. Park, J.-H. Eom, H.-A. Song, D. Seol, Y. Kim, S.-H. Shin, J. Nah, *Journal of Materials Chemistry A* **2016**, *4*, 756-763.
289. M. Coll, A. s. Gomez, E. Mas-Marza, O. Almora, G. Garcia-Belmonte, M. Campoy-Quiles, J. Bisquert, *The journal of physical chemistry letters* **2015**, *6*, 1408-1413.

290. Y. Yuan, T. J. Reece, P. Sharma, S. Poddar, S. Ducharme, A. Gruverman, Y. Yang, J. Huang, *Nature materials* **2011**, *10*, 296.
291. Z. Wang, R. Yu, C. Pan, Z. Li, J. Yang, F. Yi, Z. L. Wang, *Nature communications* **2015**, *6*, 8401.
292. J. Song, Z. Xiao, B. Chen, S. Prockish, X. Chen, A. Rajapitamahuni, L. Zhang, J. Huang, X. Hong, *ACS applied materials & interfaces* **2018**.
293. A. Sultana, P. Sadhukhan, M. M. Alam, S. Das, T. R. Middya, D. Mandal, *ACS applied materials & interfaces* **2018**, *10*, 4121-4130.
294. S. Mohammadi, A. Khodayari, *Smart Materials Research* **2012**, *2012*.
295. R. Olsen, D. Bruno, presented at the IECEC'86; Proceedings of the Twenty-first Intersociety Energy Conversion Engineering Conference, 1986 (unpublished).
296. R. B. Olsen, D. A. Bruno, J. M. Briscoe, *Journal of Applied Physics* **1985**, *58*, 4709-4716.
297. R. B. Olsen, D. A. Bruno, J. M. Briscoe, E. W. Jacobs, *Journal of Applied Physics* **1985**, *57*, 5036-5042.
298. R. Olsen, D. Brown, *Ferroelectrics* **1982**, *40*, 17-27.
299. R. Olsen, D. Bruno, J. Briscoe, J. Dullea, *Ferroelectrics* **1984**, *59*, 205-219.
300. R. B. Olsen, *Journal of Energy* **1982**, *6*, 91-95.
301. R. B. Olsen, J. M. Briscoe, D. A. Bruno, W. F. Butler, *Ferroelectrics* **1981**, *38*, 975-978.
302. R. B. Olsen, D. Evans, *Journal of applied physics* **1983**, *54*, 5941-5944.
303. G. Vats, H. S. Kushwaha, R. Vaish, N. A. Madhar, M. Shahabuddin, J. M. Parakkandy, K. M. Batoo, *Journal of Advanced Dielectrics* **2014**, *4*, 1450029.
304. A. Navid, C. S. Lynch, L. Pilon, *Smart Materials and Structures* **2010**, *19*, 055006.
305. S. Meloni, T. Moehl, W. Tress, M. Franckevičius, M. Saliba, Y. H. Lee, P. Gao, M. K. Nazeeruddin, S. M. Zakeeruddin, U. Rothlisberger, *Nature communications* **2016**, *7*, 10334.
306. C. Eames, J. M. Frost, P. R. Barnes, B. C. O'regan, A. Walsh, M. S. Islam, *Nature communications* **2015**, *6*, 7497.
307. J. Xing, Q. Wang, Q. Dong, Y. Yuan, Y. Fang, J. Huang, *Physical Chemistry Chemical Physics* **2016**, *18*, 30484-30490.
308. W. Shockley, H. J. Queisser, *Journal of Applied Physics* **1961**, *32*, 510-519.
309. J.-H. Lee, J. Kim, T. Y. Kim, M. S. Al Hossain, S.-W. Kim, J. H. Kim, *Journal of Materials Chemistry A* **2016**, *4*, 7983-7999.
310. Z. L. Wang, G. Zhu, Y. Yang, S. Wang, C. Pan, *Materials Today* **2012**, *15*, 532-543.
311. Y. Bai, T. Siponkoski, J. Peräntie, H. Jantunen, J. Juuti, *Applied Physics Letters* **2017**, *110*, 063903.
312. L. Zhu, L. Wang, C. Pan, L. Chen, F. Xue, B. Chen, L. Yang, L. Su, Z. L. Wang, *ACS Nano* **2017**.
313. K. Zhang, S. Wang, Y. Yang, *Advanced Energy Materials* **2016**.
314. Z. Wen, M.-H. Yeh, H. Guo, J. Wang, Y. Zi, W. Xu, J. Deng, L. Zhu, X. Wang, C. Hu, *Science Advances* **2016**, *2*, e1600097.
315. E. Kim, T. Park, J. Na, B. Kim, Y. Kim, H. Shin, *Solar & Alternative Energy SPIE* **2016**.
316. Z. L. Wang, J. Song, *Science* **2006**, *312*, 242-246.
317. F.-R. Fan, Z.-Q. Tian, Z. L. Wang, *Nano Energy* **2012**, *1*, 328-334.
318. Y. Yang, W. Guo, K. C. Pradel, G. Zhu, Y. Zhou, Y. Zhang, Y. Hu, L. Lin, Z. L. Wang, *Nano Letters* **2012**, *12*, 2833-2838.
319. B. Russ, A. Glaudell, J. J. Urban, M. L. Chabinyc, R. A. Segalman, *Nature Reviews Materials* **2016**, *1*, 16050.

320. Y. Zhang, J. Fang, C. He, H. Yan, Z. Wei, Y. Li, *The Journal of Physical Chemistry C* **2013**, *117*, 24685-24691.
321. J. H. Lee, K. Y. Lee, M. K. Gupta, T. Y. Kim, D. Y. Lee, J. Oh, C. Ryu, W. J. Yoo, C. Y. Kang, S. J. Yoon, *Advanced Materials* **2014**, *26*, 765-769.
322. Y. Zi, L. Lin, J. Wang, S. Wang, J. Chen, X. Fan, P. K. Yang, F. Yi, Z. L. Wang, *Advanced Materials* **2015**, *27*, 2340-2347.
323. Y. Yang, H. Zhang, G. Zhu, S. Lee, Z.-H. Lin, Z. L. Wang, *ACS Nano* **2012**, *7*, 785-790.
324. Y. Yang, Z. L. Wang, *Nano Energy* **2015**, *14*, 245-256.
325. X. Xue, S. Wang, W. Guo, Y. Zhang, Z. L. Wang, *Nano Letters* **2012**, *12*, 5048-5054.
326. H. Chang, Z.-R. Yu, *Journal of Nanoscience and Nanotechnology* **2012**, *12*, 6811-6816.
327. G. Vats, *Multi-Attribute Decision Making for Ferroelectric Materials Selection*. (Lambert Academic Publishers, 2014).
328. G. Vats, R. Vaish, *Journal of Advanced Ceramics* **2013**, *2*, 141-148.
329. G. Vats, R. Vaish, *Journal of Asian Ceramic Societies* **2014**, *2*, 5-10.
330. G. Vats, R. Vaish, *Advanced Science Focus* **2014**, *2*, 140-147.
331. G. Vats, R. Vaish, *International Journal of Applied Ceramic Technology* **2014**, *11*, 883-893.
332. G. Vats, R. Vaish, C. R. Bowen, *International Journal of Applied Ceramic Technology* **2015**, *12*, E1-E7.
333. G. Vats, M. Sharma, R. Vaish, V. S. Chauhan, N. A. Madhar, M. Shahabuddin, J. M. Parakkandy, K. M. Batoo, *Ferroelectrics* **2015**, *481*, 64-76.
334. P. Gao, M. Grätzel, M. K. Nazeeruddin, *Energy & Environmental Science* **2014**, *7*, 2448-2463.
335. A. R. b. M. Yusoff, M. K. Nazeeruddin, *The Journal of Physical Chemistry Letters* **2016**, *7*, 851-866.
336. T. M. Brenner, D. A. Egger, L. Kronik, G. Hodes, D. Cahen, *Nature Reviews Materials* **2016**, *1*, 15007.
337. D. Shi, V. Adinolfi, R. Comin, M. Yuan, E. Alarousu, A. Buin, Y. Chen, S. Hoogland, A. Rothenberger, K. Katsiev, *Science* **2015**, *347*, 519-522.
338. J. S. Yun, J. Seidel, J. Kim, A. M. Soufiani, S. Huang, J. Lau, N. J. Jeon, S. I. Seok, M. A. Green, A. Ho-Baillie, *Advanced Energy Materials* **2016**, *6*.
339. J. S. Yun, A. Ho-Baillie, S. Huang, S. H. Woo, Y. Heo, J. Seidel, F. Huang, Y.-B. Cheng, M. A. Green, *J. Phys. Chem. Lett* **2015**, *6*, 875-880.
340. J. Park, J. Huang, J. Yun, F. Liu, Z. Ouyang, H. Sun, C. Yan, K. Sun, K. Kim, J. Seidel, *Advanced Energy Materials* **2018**, 1701940.
341. Y. Cho, A. M. Soufiani, J. S. Yun, J. Kim, D. S. Lee, J. Seidel, X. Deng, M. A. Green, S. Huang, A. W. Ho-Baillie, *Advanced Energy Materials* **2018**, 1703392.
342. D. S. Lee, J. S. Yun, J. Kim, A. M. Soufiani, S. Chen, Y. Cho, X. Deng, J. Seidel, S. Lim, S. Huang, *ACS Energy Letters* **2018**, *3*, 647-654.
343. N. Faraji, C. Qin, T. Matsushima, C. Adachi, J. Seidel, *The Journal of Physical Chemistry C* **2018**, *122*, 4817-4821.
344. J. S. Yun, J. Kim, T. Young, R. J. Patterson, D. Kim, J. Seidel, S. Lim, M. A. Green, S. Huang, A. Ho-Baillie, *Advanced Functional Materials* **2018**, *28*, 1705363.
345. S. De Wolf, J. Holovsky, S.-J. Moon, P. Löper, B. Niesen, M. Ledinsky, F.-J. Haug, J.-H. Yum, C. Ballif, *The Journal of Physical Chemistry Letters* **2014**, *5*, 1035-1039.
346. K. Tvingstedt, O. Malinkiewicz, A. Baumann, C. Deibel, H. J. Snaith, V. Dyakonov, H. J. Bolink, *Scientific Reports* **2014**, *4*, 6071.
347. W. Tress, N. Marinova, O. Inganäs, M. Nazeeruddin, S. M. Zakeeruddin, M. Graetzel, *Advanced Energy Materials* **2015**, *5*.

348. H.-S. Duan, H. Zhou, Q. Chen, P. Sun, S. Luo, T.-B. Song, B. Bob, Y. Yang, *Physical Chemistry Chemical Physics* **2015**, *17*, 112-116.
349. M. Samiee, S. Konduri, B. Ganapathy, R. Kottokkaran, H. A. Abbas, A. Kitahara, P. Joshi, L. Zhang, M. Noack, V. Dalal, *Applied Physics Letters* **2014**, *105*, 153502.
350. A. Baumann, S. Väth, P. Rieder, M. C. Heiber, K. Tvingstedt, V. Dyakonov, *The Journal of Physical Chemistry Letters* **2015**, *6*, 2350-2354.
351. F. Lüdtke, N. Waasem, K. Buse, B. Sturman, *Applied Physics B* **2011**, *105*, 35.
352. G. Chanussot, V. Fridkin, G. Godefroy, B. Jannot, *Applied Physics Letters* **1977**, *31*, 3-4.
353. W. M. Lee, J. H. Sung, K. Chu, X. Moya, D. Lee, C. J. Kim, N. D. Mathur, S. W. Cheong, C. H. Yang, M. H. Jo, *Advanced Materials* **2012**, *24*.
354. A. Dhar, A. Mansingh, *Journal of Applied Physics* **1990**, *68*, 5804-5809.
355. L. Pintilie, I. Pintilie, *Materials Science and Engineering: B* **2001**, *80*, 388-391.
356. A. Glass, D. Von der Linde, D. Auston, T. Negran, *Journal of Electronic Materials* **1975**, *4*, 915-943.
357. C. W. Tang, *Applied Physics Letters* **1986**, *48*, 183-185.
358. B. Kang, B. K. Rhee, G.-T. Joo, S. Lee, K.-S. Lim, *Optics Communications* **2006**, *266*, 203-206.
359. J. W. Bennett, K. M. Rabe, *Journal of Solid State Chemistry* **2012**, *195*, 21-31.
360. P. Poosanaas, K. Uchino, *Materials Chemistry and Physics* **1999**, *61*, 36-41.
361. A. Dogan, A. Prasadarao, K. Uchino, P. Poosanaas, S. Komarneni, *Journal of Electroceramics* **1997**, *1*, 105-111.
362. S. Shannigrahi, K. Yao, *Applied Physics Letters* **2005**, *86*, 092901.
363. G. Vats, A. Kumar, N. Ortega, C. R. Bowen, R. S. Katiyar, *Energy & environmental science* **2016**, *9*, 2383-2391.
364. J. Scott, *Annual Review of Materials Research* **2011**, *41*, 229-240.
365. P. Zhao, J. Xu, H. Wang, L. Wang, W. Kong, W. Ren, L. Bian, A. Chang, *Journal of Applied Physics* **2014**, *116*, 194901.
366. A. Katti, R. Yadav, *Physics Letters A* **2017**, *381*, 166-170.
367. Q. Jiang, Y. Su, X. Ji, *Physics Letters A* **2012**, *376*, 3085-3087.
368. V. G. Karpov, D. Shvydka, *Physica Status Solidi (RRL)-Rapid Research Letters* **2007**, *1*, 132-134.
369. H. Borkar, V. Rao, S. Dutta, A. Barvat, P. Pal, M. Tomar, V. Gupta, J. Scott, A. Kumar, *Journal of Physics: Condensed Matter* **2016**, *28*, 265901.
370. H. Borkar, V. Rao, M. Tomar, V. Gupta, J. F. Scott, A. Kumar, *RSC Advances* **2017**, *7*, 12842-12855.